THE GEOLOGICAL SOCIETY OF AMERICA®

Magmatism and related metamorphism as a response to mountain-root collapse of the Dabie orogen: Constraints from geochronology and petrogeochemistry of metadiorites

Yang Yang[1], Yi-Can Liu[1,†], Yang Li[1], C. Groppo[2,3], and F. Rolfo[2,3]

[1]*Chinese Academy of Sciences, Key Laboratory of Crust-Mantle Materials and Environments, School of Earth and Space Sciences, University of Science and Technology of China, Hefei 230026, China*

[2]*Department of Earth Sciences, University of Torino, Via Valperga Caluso 35, 1-10125 Torino, Italy*

[3]*National Research Council of Italy, Institute of Geosciences and Earth Resources, Section of Torino, Via Valperga Caluso 35, 1-10125 Torino, Italy*

ABSTRACT

Post-collisional mountain-root collapse and subsequent massive partial melting occurred in the high-temperature (HT) ultrahigh-pressure (UHP) metamorphic terrane of the North Dabie complex zone (NDZ), central China. The NDZ was deeply subducted in the Triassic, producing widespread migmatites and various magmatic intrusions in the Cretaceous. Post-collisional metadiorites with distinctive large K-feldspar augen porphyroblasts, locally reported but rarely exposed in the NDZ, underwent a complex evolutional history. In this contribution, integrated studies including field investigation, petrographic observation and mineral analysis, zircon U-Pb geochronological and Hf isotopic analyses, and whole-rock elemental and Sr-Nd-Pb isotopic analyses of the metadiorites were carried out. Our results provide new constraints on the mountain-root collapse in the Dabie orogen. The metadiorites are enriched in large ion lithophile elements and light rare earth elements, whereas they are depleted in high field strength elements and heavy rare earth elements with significant Ba positive anomalies, a composition consistent with the lower continental crust. All the studied samples have moderately enriched initial $^{87}Sr/^{86}Sr$ ratios (0.707582–0.708099), low εNd(t) values (–15.3 to –20.4), and low initial Pb isotopic ratios (16.0978–16.8452, 15.3167–15.4544, and 37.1778–37.8397 for $^{206}Pb/^{204}Pb$, $^{207}Pb/^{204}Pb$, and $^{208}Pb/^{204}Pb$, respectively). However, they have highly negative εHf(t) values and Paleoproterozoic two-stage Hf model ages, which are only partially consistent with data from the associated UHP metamorphic rocks. Such features suggest the metadiorites resulted from a magma produced by mixing of Triassic UHP mafic lithologies and minor amounts of mantle-derived materials. Zircon morphological analysis and U-Pb sensitive high-resolution ion microprobe dating combined with conventional thermobarometry indicate that these upwelling melts crystallized at pressure-temperature (P-T) conditions of 5.4–5.7 kbar and 750–768 °C at ca. 130 Ma and subsequently suffered HT metamorphism at ca. 125 Ma. We conclude that the metadiorites' precursors were derived from partial melting of the Triassic subducted Neoproterozoic mafic lower-crustal rocks, with addition of minor amounts of mantle-derived materials in the Early Cretaceous, in response to mountain-root collapse of the orogen. Based on petrographic textures and mineral compositions, it is moreover inferred that formation of the distinctive K-feldspar porphyroblasts is likely related to a two-stage process, i.e., crystallization derived from biotite breakdown after the formation of the metadiorite at T = 640–703 °C and P < 4.5 kbar and coarsening related to shear deformation.

INTRODUCTION

The evolution of collisional orogens typically involves an early stage of crustal thickening and a late stage of syn-orogenic gravitational or extensional collapse (Coney and Harms, 1984; Dewey, 1988; Brown, 2001; Leech, 2001; Vanderhaeghe and Teyssier, 2001). Over-thickened crustal roots, commonly a result of plate convergence and deep crustal subduction, have been observed in several orogenic belts, e.g., the Alps (Pfiffner et al., 2000), the Himalayas (O'Brien, 2001; Myrow et al., 2003; Meissner et al., 2004), the Urals (Berzin et al., 1996; Carbonell et al., 1996), the Trans-Hudson orogen (Nelson, 1992; Baird et al., 1996), and the Dabie-Sulu orogen (Wang et al., 2000; Li et al., 2002; Yang, 2002; Xu et al., 2007). Although the over-thickened crustal roots of some old orogenic belts such as the Urals and the Trans-Hudson orogen are stable, density increase of lower crustal rocks due to metamorphic reactions (Wolf and Wyllie, 1993) generally leads to lithospheric gravitational instability and eventually results in mountain-root collapse (Kay and Kay, 1993; Rey et al., 2001; Lustrino, 2005). Hence, foundering of over-thickened mafic lower continental crust into the underlying upper mantle has been proposed as an important mechanism of lower-crustal evolution and crust-mantle material recycling (Kay and Kay, 1991, 1993; Gao et al., 2004; Lustrino, 2005), explaining the unusual average andesitic bulk composition of the continental crust (Rudnick, 1995; Rudnick and Gao, 2003). Concomitant partial melting of mountain roots generally occurs at a large-scale during collapse and produces massive post-collisional igneous intrusions and various migmatites that have been widely used as probes to trace the crustal evolution in various orogens (e.g., Martin et al., 2005; Mo et al., 2007). While the slab breakoff tectonic model has been generally applied to explain exhumation of deeply subducted crustal rocks in various orogens (e.g., Davies and von Blanckenburg, 1995; O'Brien, 2001; Liu et al., 2007b; Garzanti et al., 2018), the mountain-root collapse model has been widely used to explain post-collisional magmatism and

†Corresponding author: liuyc@ustc.edu.cn.

GSA Bulletin;
Published online 16 November 2021

https://doi.org/10.1130/B36194.1; 12 figures; 1 supplemental file.

related metamorphism (e.g., Kay and Kay, 1993; Rey et al., 2001; Lustrino, 2005; Jahn et al., 1999; Xu et al., 2007; Li et al., 2013; Garzanti et al., 2018; Yang et al., 2020).

The Dabie-Sulu orogen in central China is a typical collapsed orogen (Hacker et al., 2000; Li et al., 2002, 2013; Yang, 2002) that underwent a complex geological evolution related to continental subduction and exhumation during the Mesozoic (Xu et al., 1992, 2012b; Liu et al., 2007b, 2017; Li et al., 2020a). Here, the continental crust has been documented to have subducted to >120 km at mantle depths and then exhumed back to the surface (Okay et al., 1989; Wang et al., 1989; Xu et al., 1992). This crust was subsequently thickened to over 50 km prior to the Early Cretaceous (He et al., 2011; 2013) due to the Mesozoic collision between the South China Block (SCB) and the North China Block (NCB). However, geophysical investigations demonstrated that the present-day crustal thickness in the Dabie orogen ranges from 31 to 41 km with an average of 34 km (Gao et al., 1998; Wang et al., 2000; Schmid et al., 2001), implying that the Dabie orogen experienced an extensional tectonic collapse accompanied with lithospheric thinning and extensive magmatism in the Early Cretaceous. Geophysical evidence also suggests that eclogites are not the dominant components of the lower crust in this region. Specifically: (*i*) the P-wave velocity (V_p) of the lower crust in the Qinling-Dabie-Sulu orogen varies from 6.7 to 7.1 km/s with an average mean of 6.9 km/s (Liu and Gao, 1992; Gao et al., 1998), which is lower than that of the global continental crust (7.14 km/s, Rudnick and Fountain, 1995) and of the North Dabie complex zone (NDZ) eclogites (7.9–8.2 km/s), and (*ii*) the Poisson's ratio (V_p/V_s) of the lower crust and upper mantle in the Dabie orogen (0.27–0.28, Gao et al., 1998) is higher than that of the NDZ eclogites (0.21–0.24).

In the NDZ, the Early Cretaceous post-collisional magmatism produced various igneous rocks (Jahn et al., 1999; Li et al., 1999; Chen et al., 2002; Bryant et al., 2004; Zhao et al., 2005, 2007). These lithologies predominantly consist of felsic granitoid intrusions (Chen et al., 2002; Wang et al., 2007; Xu et al., 2007, 2012a; Zhao et al., 2007) with minor mafic-ultramafic plutons (Jahn et al., 1999; Li et al., 1999; Zhao et al., 2005; Huang et al., 2007). Among felsic lithologies, adakitic granites with formation ages of less than 130 Ma are characterized by significantly lower Sr/Y, Sr/CaO, $(La/Yb)_N$, and $(Dy/Yb)_N$ ratios compared to previous granitoid intrusions emplaced at 143–130 Ma (He et al., 2011). These compositional variations observed before and after ca. 130 Ma are considered to be due to a change of the anatectic source during the removal of crustal roots (Ma et al., 2003; Xu et al., 2007; He et al., 2011; Li et al., 2013). Mafic-ultramafic plutons in the NDZ were emplaced at 123–130 Ma (Hacker et al., 1998; Li et al., 1999; Wang and Deng, 2002). Although these lithologies (e.g., gabbro, pyroxenite, and hornblendite) display typical "continental" geochemical features, previous studies suggest their precursors were mixed with mantle-sourced materials (Jahn et al., 1999; Zhao et al., 2005; Huang et al., 2007). Chemically intermediate lithologies such as (meta)diorites have received much less attention in the NDZ due to their scattered occurrence. New metadiorite bodies have been identified in this study; these rocks provide an opportunity to better explore the tectonic significance of post-collisional magmatism and related mountain-root collapse of the Dabie orogen in the Cretaceous. Here, we present a comprehensive study of these metadiorites combining petrographic observation and mineral analysis, whole-rock major-trace elements and Sr-Nd-Pb isotopes, and zircon U-Pb ages and Hf isotopes, in order to place new constraints on the process of mountain-root collapse of the orogen.

GEOLOGICAL SETTING AND SAMPLES

The North Dabie Complex Zone

The Dabie orogen is located in the intermediate segment of the Qinling-Dabie-Sulu orogenic belt (Fig. 1A), which was formed as the result of northward subduction of the SCB beneath the NCB in the Triassic (Xu et al., 1992; Li et al., 1993). As one of the most famous and well-preserved ultrahigh-pressure (UHP) metamorphic terranes in the world, the Dabie orogen contains different lithologies which experienced various metamorphic grades and evolutional histories (Liu and Li, 2008; Xu et al., 2012b; Liu et al., 2017; Li et al., 2020a). It can be subdivided into five lithotectonic units from south to north separated by faults (Xu et al., 2003, 2005; Liu et al., 2007a): (1) the Susong complex zone (SZ); (2) the South Dabie low-temperature (T) eclogite zone (SDZ); (3) the Central Dabie mid-T/UHP metamorphic zone (CDZ); (4) the North Dabie high-T/UHP complex zone (NDZ); and (5) the Beihuaiyang zone (BZ) (Fig. 1B). Among them, the SDZ, CDZ, and NDZ are three eclogite-bearing units that experienced UHP metamorphism during the Triassic subduction (Xu et al., 2003; Li et al., 2004, 2020a; Rolfo et al., 2004; Malaspina et al., 2006; Liu et al., 2007a, 2011b).

The NDZ is located between the BZ and CDZ, bounded by the Xiaotian-Mozitan fault to the north, the Wuhe-Shuihou fault to the south, and the Shangcheng-Macheng fault to the west (Fig. 1B). In comparison with the other two eclogite-bearing units, the NDZ underwent multistage high-T metamorphic events, including a long-term high-T granulite-facies metamorphic overprint after eclogites-facies metamorphism during the initial stages of exhumation (Liu et al., 2011b, 2015; Groppo et al., 2015; Deng et al., 2019; Li et al., 2020b), and widespread partial melting and migmatization concomitant with the emplacement of abundant Cretaceous granites and associated intrusions (Wang et al., 2002; Liu et al., 2007b; Wu et al., 2007b; Wang et al., 2013; Xu and Zhang, 2017; Yang et al., 2020). The NDZ mainly consists of tonalitic and granitic orthogneisses (locally migmatitic) and post-collisional Cretaceous intrusions, with subordinate meta-peridotite, garnet-bearing amphibolite, granulite, and eclogite. Geochronological studies in this region demonstrated that the precursors of migmatites and meta-igneous rocks (including granitic orthogneiss and eclogites) are Neoproterozoic in age (Liu et al., 2007a, 2007b, 2011a; Yang et al., 2020). Most metamorphic lithologies in the NDZ underwent pervasive retrogression and deformation during deep subduction and subsequent exhumation in the Mesozoic (Xu et al., 2003, 2005; Liu et al., 2005, 2007a, 2011a; Malaspina et al., 2006), such that the mineral assemblages mainly reflect amphibole-facies conditions, whereas granulite-facies and eclogites-facies relics are only rarely preserved.

The Early Cretaceous thermal overprint played a crucial role in the NDZ, producing large-scale partial melting, migmatization (Wang et al., 2013; Yang et al., 2020), and accompanying post-collisional magmatism (Jahn et al., 1999; Li et al., 1999; Bryant et al., 2004; Zhao et al., 2005, 2007). As a result, the NDZ shows a great variety of migmatites with different types of leucosomes (Wang et al., 2013; Yang et al., 2020) and various magmatic bodies intruded into the UHP granitic orthogneisses and related rocks. These post-collisional igneous intrusions are dominantly represented by Cretaceous granitoids (Chen et al., 2002; Xu et al., 2007, 2012a; Zhao et al., 2007) with subordinate mafic-ultramafic rocks (Jahn et al., 1999; Li et al., 1999; Zhao et al., 2005; Huang et al., 2007), while chemically intermediate intrusions such as diorites are rarely reported.

Petrography and Mineral Chemistry

The studied metadiorites outcrop sporadically in the NDZ, and generally exhibit conspicuous deformation with distinct foliations. Eight metadiorite samples were collected in seven localities as shown in Figure 1C. Representative field photographs are provided in Figure 2. The metadio-

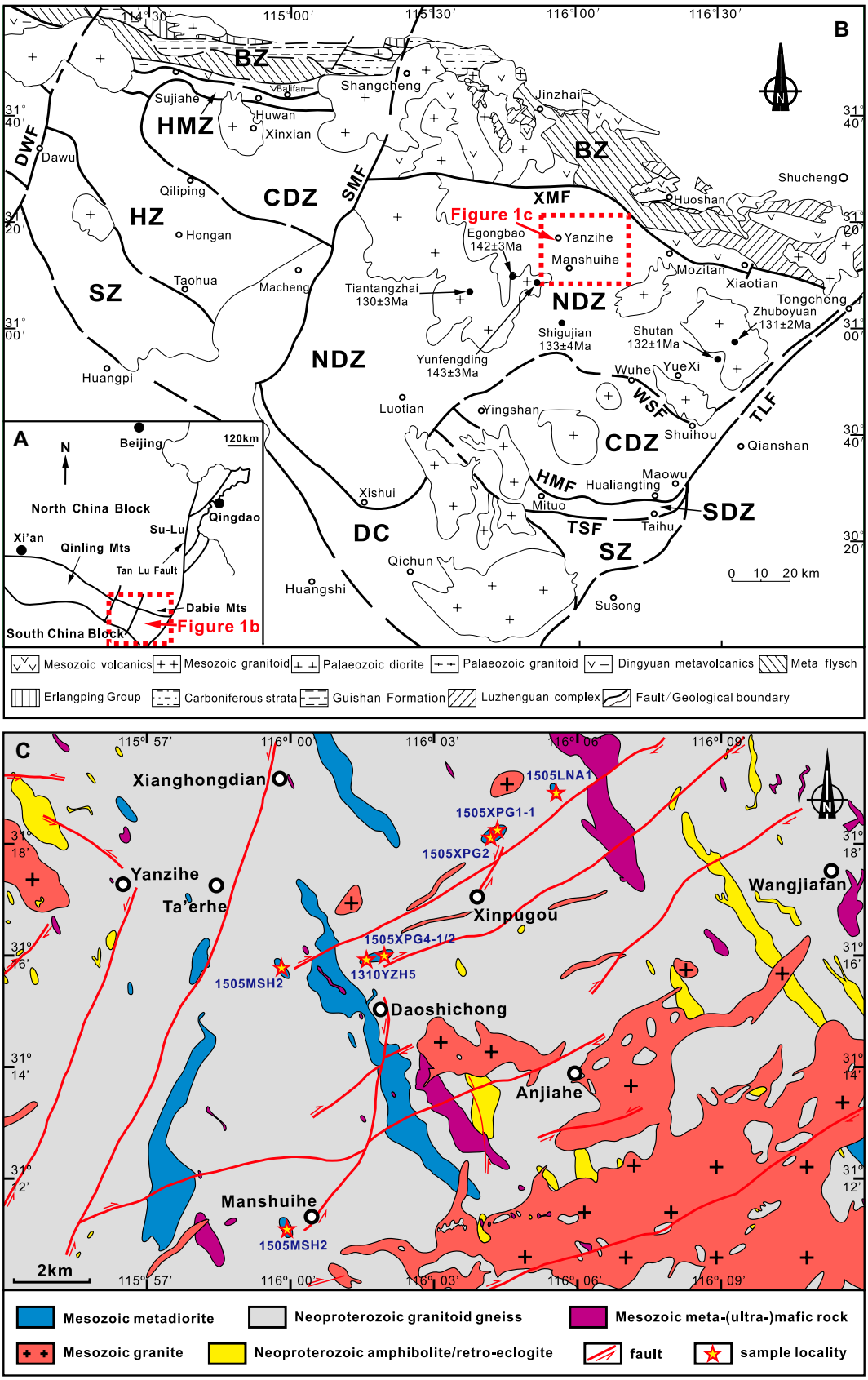

Figure 1. Geological map showing the study area. (A) Location of the Dabie orogen within the Triassic Qinling-Dabie-Sulu collision orogen in central China; (B) lithotectonic units of the Dabie orogen (modified from Liu et al., 2007a); (C) the metadiorites and related rocks around sample localities in the North Dabie complex zone. BZ—Beihuaiyang zone; NDZ—North Dabie complex zone; CDZ—Central Dabie ultrahigh-pressure metamorphic zone; SDZ—South Dabie low-temperature eclogite zone; SZ—Susong complex zone; HMZ—Huwan mélange zone; HZ—Hong'an low-temperature eclogite zone; DC—amphibolite-facies Dabie complex; XMF—Xiaotian-Mozitan fault; WSF—Wuhe-Shuihou fault; HMF—Hualiangting-Mituo fault; TSF—Taihu-Shanlong fault; TLF—Tan-Lu fault; SMF—Shangcheng-Macheng fault; DWF—Dawu fault. Geochronological data for Cretaceous granites and mafic-ultramafic intrusive rocks are from Xue et al. (1997), Hacker et al. (1998), Jahn et al. (1999), Bryant et al. (2004), Zhao et al. (2005), and Wang et al. (2007).

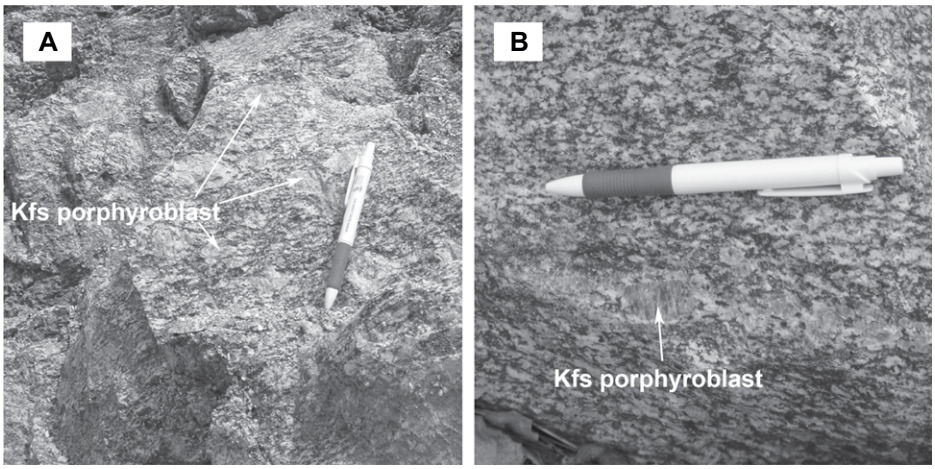

Figure 2. Field photographs of metadiorites with large K-feldspar (Kfs) augen porphyroblasts from the North Dabie complex zone in central China.

rites are generally found tectonically in contact with the orthogneisses that underwent multistage metamorphic evolution related to Late Triassic deep subduction (Liu et al., 2007b) followed by multiple anatexis and migmatization events during exhumation and post-orogenic collapse (Yang et al., 2020). The metadiorite dykes or blocks are several meters in width and length and they are exposed in different localities. The rocks are generally deformed and strongly metamorphosed with orientation of minerals such as feldspar and amphibole; they have a porphyroblastic texture (Fig. 2), but they lack migmatitic textures (e.g., leucosomes and melanosomes) typical of the migmatites in the region, suggestive of their different genesis and evolutional history. The metadiorites are mainly composed of amphibole (20 vol%), biotite (10 vol%), K-feldspar (30 vol%), plagioclase (20 vol%), quartz (20 vol%), and accessory minerals (<1 vol%) such as allanite, apatite, zircon, and magnetite; typically, K-feldspar occurs as porphyroblasts. K-feldspar porphyroblasts are coarse-grained, idiomorphic, and generally surrounded by a white corona consisting of plagioclase and quartz. Average grain size of most rock-forming minerals varies in the range from 0.3 to 1.0 mm, whereas Kfs porphyroblasts can reach 15 mm. The modal abundance of the porphyroblasts is highly variable among different samples, and they are generally oriented parallel to the main foliation.

Amphiboles occasionally occur as large subhedral crystals several millimeters across (Figs. 3A and 3B). Two groups of amphiboles can be distinguished by their different compositions (especially Ti contents) and colors (i.e., green and brown under plane polarized light) (Figs. 3C and 3D). Both groups are calcic amphiboles according to the classification of Leake et al. (1997) and plot in the magnesiohornblende or tschermakite fields with X_{Mg} values ranging from 0.58 to 0.66. Brown amphiboles (Amp1) are rare and generally occur as fine grains included in other minerals (such as ilmenite); they display higher Ti (0.168–0.174 atoms per formula unit [a.p.f.u.]) and Al^{IV} (1.552–1.631 a.p.f.u.) contents, suggesting higher T formation conditions (Raase, 1974) (Fig. 4A). Green amphiboles (Amp2) are generally dominant both in size and quantity and have lower Ti (0.115–0.145 a.p.f.u.) and Al^{IV} (1.388–1.515 a.p.f.u.) contents (Fig. 4A). Green amphiboles from samples 1310YZH5 and 1505LNA1 are slightly zoned (Table S1[1]) and display similar decrease of Al^{IV} contents from core to rim, suggestive of decompression during crystallization.

Biotites generally occur as inclusions in amphibole and K-feldspar grains (Figs. 3B and 3E) as well as flakes in the matrix (Figs. 3A and 3F). They are characterized by high FeO_T (17.43–19.21 wt%) and TiO_2 (4.54–5.36 wt%) contents. They are relatively rich in Mg with molar Mg/(Mg + Fe) values of 0.51–0.57. Moreover, they do not show any distinct compositional differences in the various textural domains.

[1]Supplemental Material. Table S1: Electron microprobe analyses (wt%) of representative minerals in the NDZ metadiorites; Table S2: Major and trace elements concentrations of the NDZ metadiorites; Table S3: Zircon SHRIMP U-Pb isotopic compositions of the NDZ metadiorites; Table S4: Zircon REE concentrations of sample 1310YZH5 from the NDZ; Table S5: Zircon Lu-Hf isotopic compositions of the NDZ metadiorites; Table S6: Whole-rock Rb-Sr, Sm-Nd, and Pb isotopic data of the NDZ metadiorites; Table S7: P-T estimates of the NDZ metadiorites. Please visit https://doi.org/10.1130/GSAB.S.16859710 to access the supplemental material, and contact editing@geosociety.org with any questions.

Feldspar is a widespread mineral with variable composition and textural occurrence. The K-feldspar (Kfs) in the studied samples can be subdivided into four groups as a function of different textural domains: (1) Kfs grains in the matrix (Figs. 3G and 3H); (2) Kfs inclusions in plagioclase or amphibole (Fig. 3I); (3) large Kfs porphyroblasts (Fig. 3J); and (4) Kfs grains in myrmekites or coronas around Kfs porphyroblasts (Figs. 3K and 3L). The Kfs grains (Fig. 4B) in the matrix have the highest and most variable potassium contents (anorthite[An]$_{0–1}$[albite]Ab$_{1–8}$[orthosite]Or$_{92–99}$), and are generally associated with plagioclase, quartz, and biotite. Kfs inclusions in plagioclase (Fig. 4B) and amphibole are homogeneous in composition ($An_{0–1}Ab_{10–11}Or_{89–90}$) and often coexist with quartz. Kfs porphyroblasts (Fig. 4B) are homogeneous with a composition of $An_{0–1}Ab_{14–19}Or_{80–86}$ and display the highest X_{ab} and lowest X_{or} values among all types of Kfs. The cores of Kfs porphyroblasts are almost devoid of mineral inclusions, while the rims are significantly richer in mineral inclusions. The Kfs grains in myrmekites or coronas around the porphyroblasts (Fig. 4B) have similar compositions ($An_{0–1}Ab_{12–15}Or_{85–88}$) compared with the porphyroblasts but have lower X_{ab} and are generally associated with plagioclase and quartz.

Plagioclase also occurs in various textural domains: (1) in the matrix (Figs. 3G and 3H), (2) as inclusions in biotite, amphibole, and Kfs porphyroblasts (Fig. 3E), and (3) in myrmekites or coronas around the Kfs porphyroblasts (Figs. 3K and 3L). Plagioclase composition is constant within a single sample, while systematic compositional differences occur between different samples, related to the characters of the protoliths. For example, plagioclase crystals in sample 1505LNA1 have average compositions of $An_{27–29}Ab_{69–72}Or_{1–2}$, which is systematically sodium-richer than plagioclase in sample 1310YZH5 ($An_{29–31}Ab_{67–69}Or_2$) (Fig. 4C).

ANALYTICAL METHODS

Whole-Rock Major and Trace Element Analyses

Whole-rock major and trace element compositions were determined at Langfang Laboratory of Geophysical Exploration, Geological Exploration Bureau of Hebei Province, Ministry of Land and Mineral Resources of China. Eight samples were first ground in an agate mill to <200 mesh for major and trace element analysis. Loss on ignition, FeO, and Fe_2O_3 were determined by gravimetric, volumetric, and titrimetric methods, whereas other major elements were determined by X-ray fluorescence spectrometry with analytical precision better than 1%. About 50 mg

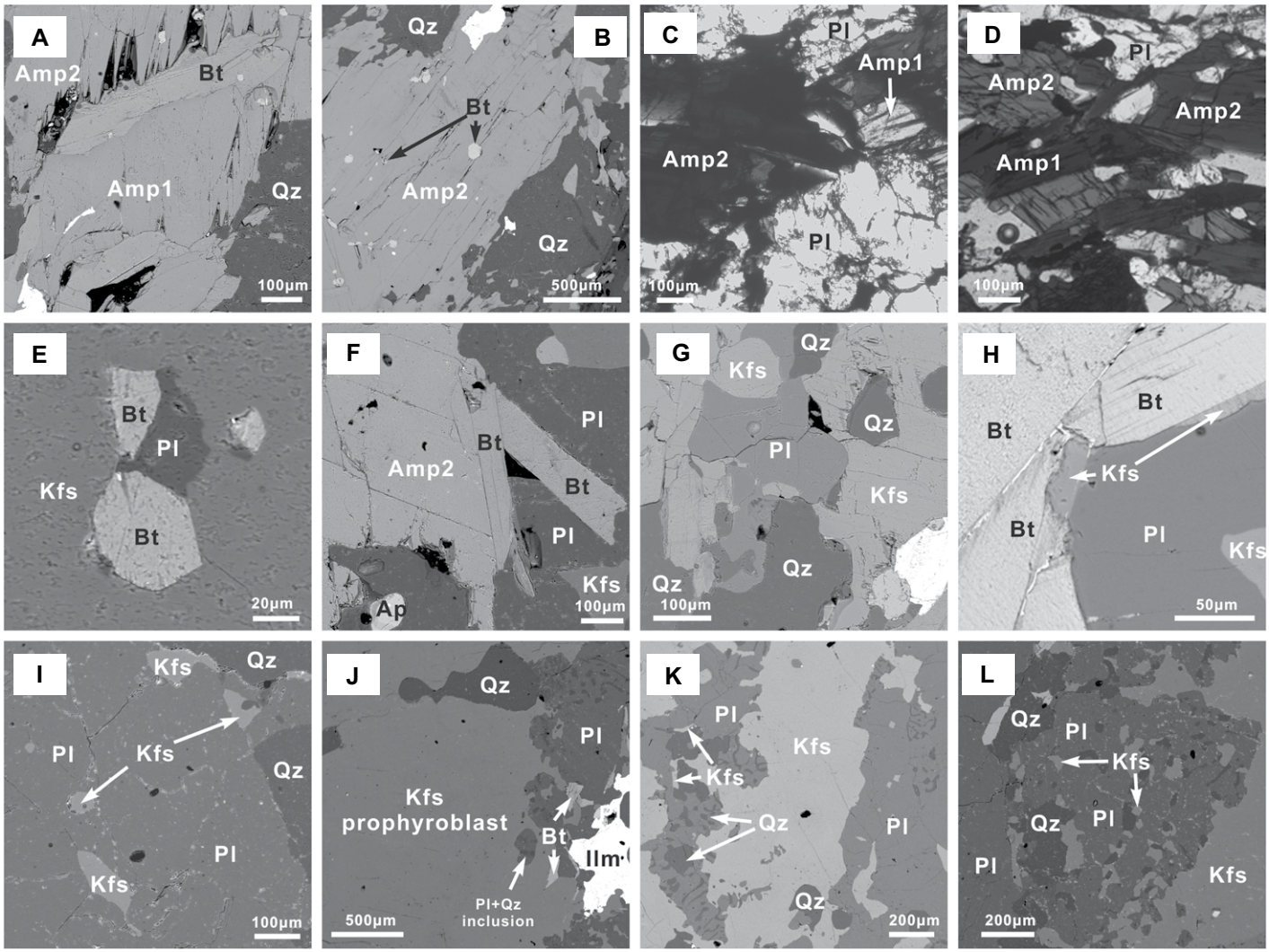

Figure 3. Photomicrographs and backscattered electron images of metadiorites in the North Dabie complex zone in central China. (A) Brown amphibole (Amp1) coexisting with biotite (Bt) and quartz (Qz) in matrix; (B) green amphibole (Amp2) in matrix with euhedral biotite inclusions; (C and D) green amphibole (Amp2) and brown amphibole (Amp1); (E) primary inclusion consist of Bt + plagioclase (Pl) in core of K-feldspar (Kfs) porphyroblast; (F) biotite display as flakes coexisting with amphibole and plagioclase in matrix; (G) Kfs grains coexisting with plagioclase and quartz in matrix; (H) Kfs films between biotite and plagioclase in the matrix; (I) Kfs inclusions in plagioclase; (J) large Kfs porphyroblasts with secondary Pl + Qz inclusions in the rim, surrounded by Pl + Qz myrmekites/coronas; (K and L) Kfs grains in myrmekites and coronas around the Kfs porphyroblasts. Ilm—ilmenite.

powders of each sample were accurately weighed and dissolved in a 1:1 mixture of HF + HNO_3 at 190 °C using Parr bombs for ~72 h, and complete sample dissolution was achieved. The dissolved samples were diluted to 50 mL using 1% HNO_3 before analysis. Trace element analyses were accomplished using an inductively coupled plasma–mass spectrometer. Analytical precisions for trace elements are better than 5% (2σ).

Zircon U-Pb Dating

Zircons in the NDZ metadiorites were separated from ~1–3 kg of each sample. After crushing and sieving, zircons were chosen by magnetic and heavy liquid separation and hand-picked under a binocular microscope at Langfang Laboratory of Geophysical Exploration, Geological Exploration Bureau of Hebei Province, Ministry of Land and Mineral Resources. After that, zircon grains were further selected by hand-picking under a binocular microscope, and mounted in an epoxy mount, which was polished to section the crystals for analyses, with a zircon U-Pb standard transmission electron microscope (417 Ma) (Black et al., 2003) at the Beijing SHRIMP Center, Chinese Academy of Geological Sciences (CAGS). Internal zoning patterns of crystals were observed by cathodoluminescence (CL) images.

Zircon U-Pb dating was undertaken on four samples by the SHRIMP II at the Beijing SHRIMP Centre, CAGS, with transmitted and reflected light micrographs and CL images as a guide to selection of U-Pb dating spots. The detailed analytical method was described by Compston et al. (1984) and Williams (1998). Common Pb was corrected using the measured ^{204}Pb. The U-Pb isotope data were treated following Compston et al. (1984) with the ISOPLOT program of Ludwig (2003).

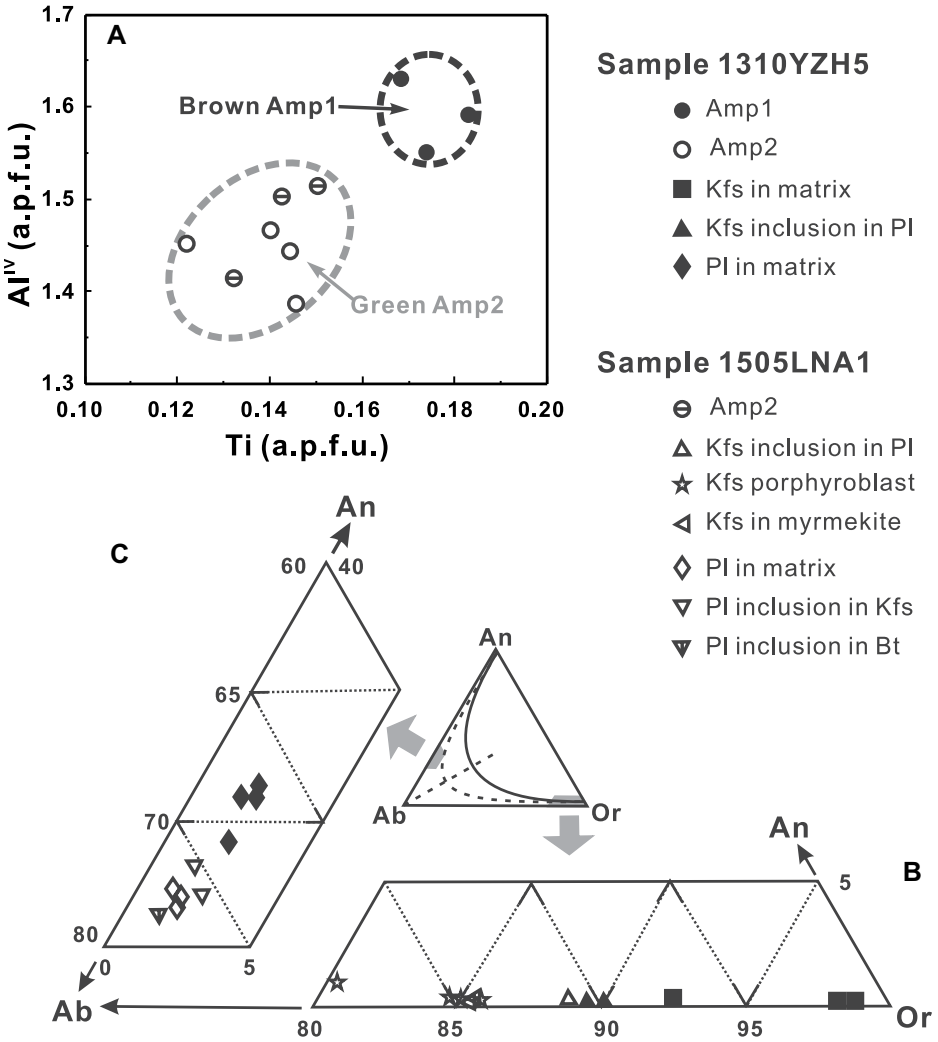

Figure 4. Compositions of representative minerals in the metadiorites from the North Dabie complex zone in central China. (A) Ti versus Al^{IV} contents diagram of brown amphibole (Amp1) and green amphibole (Amp2); (B) K-feldspars (Kfs) in the anorthite-albite-orthosite (An-Ab-Or) ternary diagram; (C) plagioclases in the An-Ab-Or ternary diagram. Pl—plagioclase; Bt—biotite; a.p.f.u.—atoms per formula unit.

Zircon Trace Element Analyses

Zircon trace element concentrations were performed by a laser ablation–inductively coupled plasma–mass spectrometer at the Chinese Academy of Sciences (CAS), Key Laboratory of Crust-Mantle Materials and Environments, University of Science and Technology of China, Hefei, China. NIST glasses 610 and 612 were selected as external calibration standards for trace element analyses. Off-line evaluation and integration of signal to background, time-drift correction, quantitative calibration, and common-lead correction were processed with the ICPMSDataCal software (Liu et al., 2008, 2010). More details about the laser-ablation technique are given in Liu et al. (2007c).

Zircon Hf Isotopic Analyses

Zircon in situ Hf isotopes were measured by a Neptune (Plus) multicollector–inductively coupled plasma–mass spectrometer attached to a New Wave ArF 193 nm laser ablation system at State Key Laboratory for Mineral Deposits Research, Nanjing University, China. A beam diameter of ~55 μm with repetition time of 10 Hz and laser energy of 15J/cm^2 was used in the laser ablation microprobe analyses and zircon powder was carried by Ar and He carrier gas. Repeated measurements on the Mud Tank Hf standard yielded $^{176}Hf/^{177}Hf$ values of 0.282492 ± 12 (2σ), identical to the recommended value of 0.282500 ± 50 (2σ). Chondritic values of Blichert-Toft and Albarède (1997) were used to calculate the $\varepsilon_{Hf}(t)$ values of the samples, while the two-stage depleted mantle (DM) model ages were calculated basing on the DM values of Griffin et al. (2000).

Whole-Rock Rb-Sr, Sm-Nd, and Pb Isotopic Analyses

Chemical treatment and measurement of whole-rock Rb-Sr, Sm-Nd, and Pb isotopes were performed at the CAS Key Laboratory of Crust-Mantle Materials and Environments, University of Science and Technology of China, Hefei. Sample powder was weighed and mixed with ^{87}Rb-^{84}Sr and ^{147}Sm-^{150}Nd spikes prior to dissolution in concentrated HF-HNO_3 for one week in a clean laboratory. Chemical separation was performed on conventional ion exchange resin columns. Rb-Sr, Sm-Nd, and Pb contents and isotopic ratios were measured on a multicollector Finnigan MAT-262 thermal ionization mass spectrometer in static mode in the Laboratory for Radiogenic Isotope Geochemistry, University of Science and Technology of China, Hefei. The Sr and Nd isotope ratios were normalized to $^{86}Sr/^{88}Sr = 0.1194$ and $^{146}Nd/^{144}Nd = 0.7219$, respectively, to correct for mass fractionation. During the data collection period, repeated measurements on the NBS987 Sr standard solution yielded an average $^{87}Sr/^{86}Sr$ value of 0.710239 ± 12 (2σ), and the La Jolla Nd standard solution gave an average $^{143}Nd/^{144}Nd$ value of 0.511870 ± 8 (2σ) (Chen et al., 2000, 2007). Accuracy was estimated to be better than 0.5% and 1.0% for Sm and Rb, respectively. Mass dependent fraction for Pb isotope ratios was 0.1% per atomic mass unit based on repeated analyses of NBS 981 standard measurements (Chen et al., 2000, 2007).

Mineral Composition Analysis

Mineral compositions were measured in the experimental center at the School of Resources and Environmental Engineering, Hefei University of Technology with a JXA-8230 electron microprobe using an operation condition of 15 kV accelerating voltage. The analysis was performed using a specimen current of 20 nA and beam diameter of 3 μm. The accuracy and precision of most elements was estimated to be better than 2%. Mineral abbreviations through the text including figures and tables are after Whitney and Evans (2010).

RESULTS

Whole-Rock Major and Trace Elements

The results of whole-rock major and trace element analyses for the eight selected metadiorite

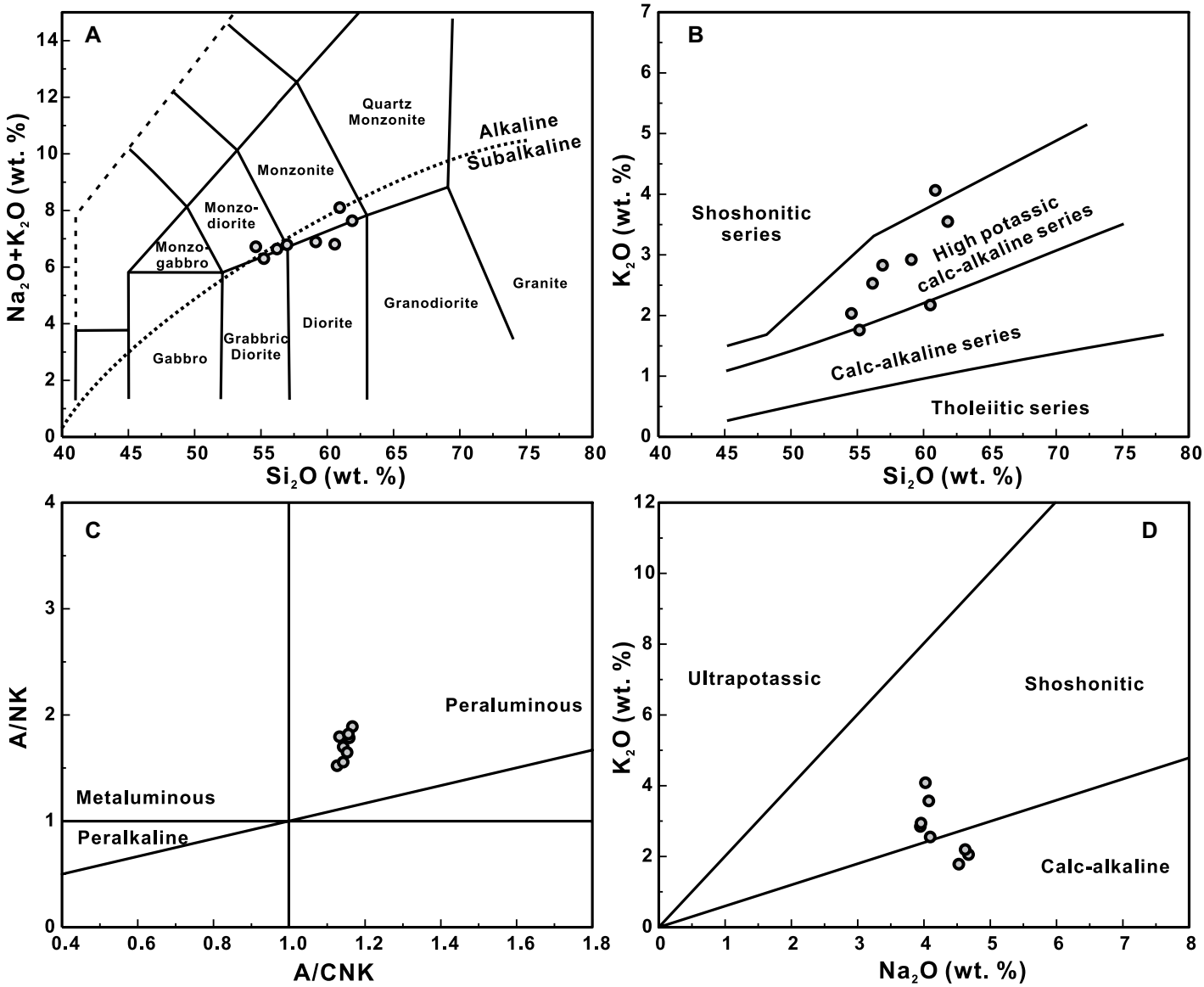

Figure 5. Major-element scatter diagrams of the metadiorites from the North Dabie complex zone in central China. (A) ($Na_2O + K_2O$) versus SiO_2 diagram; (B) SiO_2 versus K_2O diagram; (C) A/CNK (molar $Al_2O_3/[CaO + Na_2O + K_2O]$) and A/NK (molar $Al_2O_3/[Na_2O + K_2O]$) diagram; (D) Na_2O versus K_2O diagram.

samples are presented in Supplementary Table S2 (see footnote 1). The metadiorites have homogeneous magnesian compositions with intermediate SiO_2 (54.60–61.87 wt%) and MgO (2.23–3.91 wt%) contents and $Mg^{\#}$ values ranging from 44.20 to 50.35. The ($Na_2O + K_2O$) versus SiO_2 and K_2O versus SiO_2 diagrams (Figs. 5A and 5B) indicate that most of the metadiorites fall within the subalkaline series and high-K calc-alkaline series fields, respectively, with high K_2O (1.77–4.07 wt%) and Na_2O (39.5–4.67 wt%) contents and low Na_2O/K_2O ratios (1.50–3.89). All the samples are slightly peraluminous (Fig. 5C) with A/CNK (molar $Al_2O_3/[CaO + Na_2O + K_2O]$) and A/NK (molar $Al_2O_3/[Na_2O + K_2O]$) values ranging from 1.13 to 1.17 and 1.57–1.90, respectively, high Al_2O_3 (16.52–18.11 wt%) and low TiO_2 (0.75–1.07 wt%), FeO_T (4.76–7.30 wt%) and CaO (4.30–6.35 wt%) contents.

The trace elements display high Sr/Y ratios (33.83–67.31), with high Sr (813.56–1241.79 ppm) and low Y (12.43–25.62 ppm) contents (Fig. 6). Nb/Ta ratios are high (17.23–30.49), while the Nb/La ratios (0.16–0.38) are relatively low. Chondrite-normalized rare earth elements (REE) diagram (Boynton, 1984) indicates a slightly light (L)REE over heavy (H) REE enrichment with HREE depletion and high $(La/Yb)_N$ ratios (11.80–26.91) (Fig. 7A). No discernible middle (M)REE depletion and Eu anomaly were observed with $(Dy/Yb)_N$ ratios and δ_{Eu} values ranging from 1.14 to 1.54 and from 0.81 to 1.04, respectively. In addition, the primitive mantle normalized trace elements diagram (Sun and McDonough, 1989) suggests the metadiorites are enriched in large ion lithophile elements (LILEs, e.g., Rb, Sr, Ba, K, and Pb), but depleted in high-field strength elements (HFSEs, e.g., Nb, Ta, and Ti), whereas Zr and Hf exhibit no significant depletion (Fig. 7B).

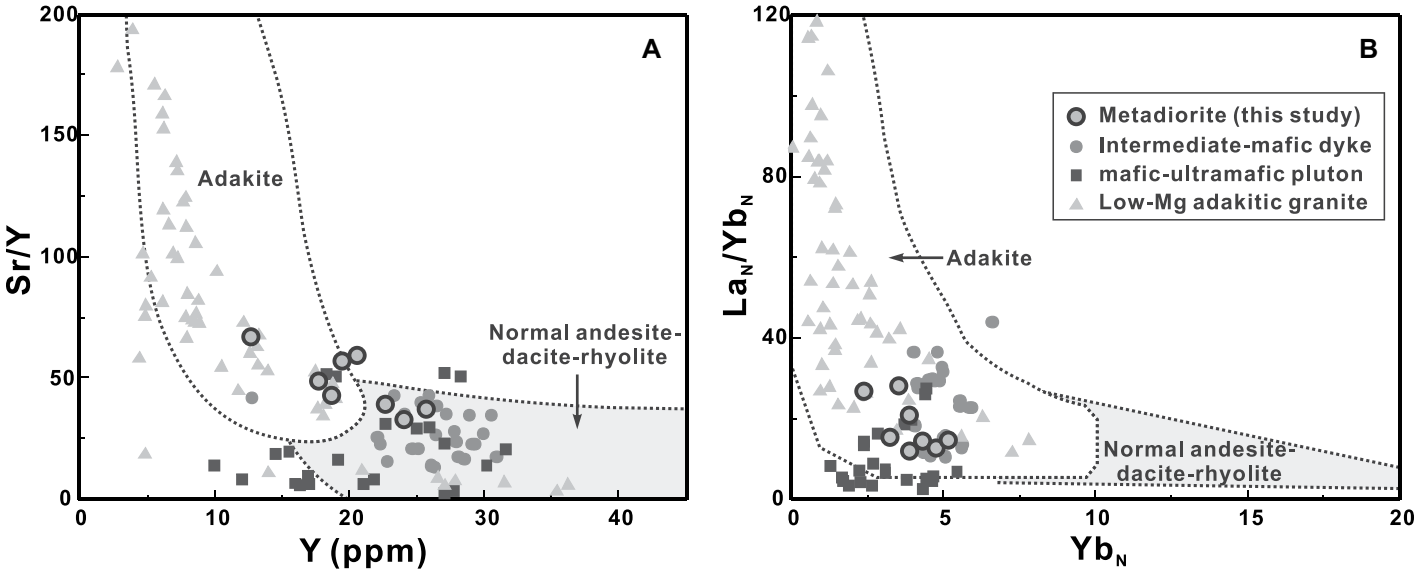

Figure 6. Binary plots of trace element compositions for metadiorites in the North Dabie complex zone (NDZ) in central China (modified after Defant and Drummond, 1990; Atherton and Petford, 1993). (A) Y versus Sr/Y diagram; (B) Yb_N versus La_N/Yb_N diagram. Normalized values of rare earth elements are from Sun and McDonough (1989). Data sources: other Early Cretaceous intermediate-mafic dykes in the NDZ from Wang et al. (2005) and Xu et al. (2013); Early Cretaceous low-Mg adakitic granites in the NDZ from Wang et al. (2007) and Xu et al. (2013); Early Cretaceous mafic-ultramafic dykes in the NDZ from Wang et al. (2005), Zhao et al. (2005), and Huang et al. (2007).

Zircon Morphology and U-Pb Dating

Zircon grains from four samples were selected for zircon sensitive high-resolution ion microprobe (SHRIMP) U-Pb dating. The obtained results are summarized in Supplementary Table S3 (see footnote 1) and the CL images of representative zircons are reported in Figure 8.

Zircons from sample 1310YZH5 are subhedral to euhedral, prismatic, and colorless, ranging in size from 70 to 300 μm with aspect ratios of 2:1–5:1 (Figs. 8A–8D). CL images reveal a core-rim texture (e.g., Figs. 8C and 8D). The prismatic cores exhibit clear oscillatory zoning with high Th/U ratios (0.74–1.37), suggesting a magmatic genesis (Rubatto and Gebauer, 2000), while the light-gray overgrowth rims are characterized by homogeneous structure and relatively low Th/U ratios (0.44–0.92, most <0.65), typical of metamorphic zircons (Corfu et al., 2003). Results of 17 analytical spots on the zircon cores and five spots on the rims on or near the concordia line define weighted mean $^{206}Pb/^{238}U$ ages of 129 ± 1 Ma (mean square weighted deviation [MSWD] = 1.70) and 127 ± 2 Ma (MSWD = 1.09), respectively (Fig. 9A).

Zircons from sample 1505LNA1 are prismatic to equant, colorless and translucent, and exhibit similar core-rim texture as sample 1310YZH5 (Figs. 8E–8H). Most zircons are euhedral, with gray oscillatory zoning prismatic cores and thin or even invisible overgrowth rims (e.g., Figs. 8G and 8H); grain lengths range from 100 to 400 μm and aspect ratios are ~3:1. Few zircon grains have light thick overgrowth rims surrounding perfect or embayed cores, displaying prismatic or equant features. Zircon rims with low uranium contents (104–159 ppm) are generally homogeneous and have slightly lower Th/U ratios (0.46–0.81) compared to the oscillatory cores. Thirteen analytical spots of zircon cores gave a weighted mean $^{206}Pb/^{238}U$ age of 131 ± 1 Ma (MSWD = 0.80) and three spots of homogeneous rims yielded a weighted mean age of 124 ± 2 Ma (MSWD = 0.25) (Fig. 9B).

Zircons from sample 1505MSH2 are euhedral to anhedral, prismatic to equant, colorless, and translucent with lengths up to 500 μm and aspect ratios ranging from 1:1 to 4:1 (Figs. 8I–8L). Most zircon grains display typical core-rim texture while some oscillatory cores are embayed or truncated by gray homogeneous rims (e.g., Figs. 8J and 8L); a few of the zircon grains retain no obvious magmatic cores. Thirteen zircon cores with oscillatory zoning and two homogeneous rims gave concordia weighted mean $^{206}Pb/^{238}U$ ages of 133 ± 1 Ma (MSWD = 0.94) and 126 ± 3 Ma (MSWD = 0.50), respectively (Fig. 9C).

Zircons from sample 1505XPG1-1 are euhedral to anhedral, prismatic, colorless, and translucent (Figs. 8M–8P). Typical zircon grains have length and aspect ratios varying from 100 to 300 μm and from 1:1 to 6:1, respectively. They occasionally exhibit oscillatory zoned or homogeneous prismatic cores and thin overgrowth rims (e.g., Figs. 8O and 8P); a few of the grains display corrosion structures. Nine zircon cores with high Th/U ratios (0.49–1.43) gave concordia weighted mean $^{206}Pb/^{238}U$ ages of 132 ± 2 Ma (MSWD = 2.1) while one rim analytical spot with a low Th/U ratio of 0.47 yielded a concordia $^{206}Pb/^{238}U$ age of 122 ± 2 Ma (Fig. 9D).

Zircon Trace Elements

Representative trace element contents of zircon cores and rims in the NDZ metadiorite (sample 1310YZH5) are listed in Supplementary Table S4 (see footnote 1). Zircon cores have identical steep HREE patterns with positive Ce anomalies values and negative Eu anomalies (δ_{Eu} = 0.35–0.53), high total REE contents (343.26–807.61 ppm), and slightly lower Lu_N/Dy_N values (6.85–8.75). Zircon rims exhibit similar REE patterns (with δ_{Eu} values of 0.32–0.66) with cores except for the relatively lower REE contents with values ranging from 214.59 to 319.10 ppm and higher Lu_N/Dy_N values (10.85–12.47) (Fig. 7C).

Zircon Hf Isotopes

Three samples (1310YZH5, 1505LNA1, and 1505XPG1-1) were selected for in situ zircon Hf isotopic analysis and the details are summarized in Supplementary Table S5 (see footnote 1). All the analyzed zircons from the three samples have $^{176}Lu/^{177}Hf$ ratios of 0.000416–0.001195,

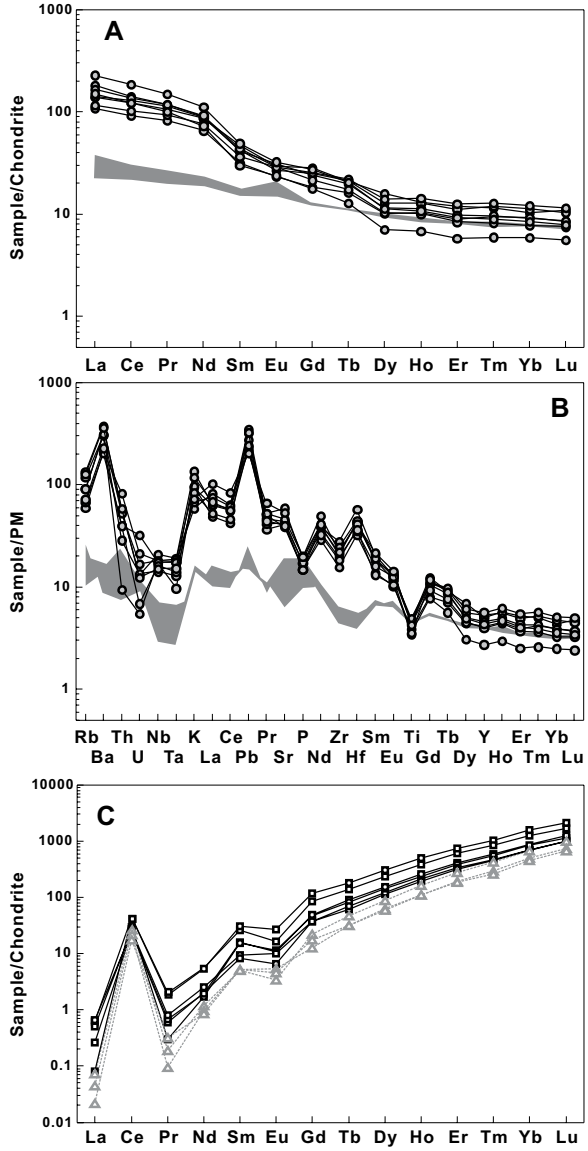

Figure 7. Whole-rock chondrite-normalized rare earth element (REE) patterns (A) and corresponding primitive mantle (PM)-normalized trace element patterns (B), and zircon core-rim chondrite-normalized REE patterns (C) for metadiorites in the North Dabie complex zone in central China. Normalized values of REEs and trace elements are from Boynton (1984) and Sun and McDonough (1989), respectively. Gray fields represent data for the eclogites in this region from Gu (2012). Black circles filled with gray stand for whole-rock element contents in A and B, while black squares and gray triangles are representative of zircon cores and rims in C, respectively.

0.000219–0.001274, and 0.000470–0.001449, respectively. Low $^{176}Lu/^{177}Hf$ ratios (<0.002) suggest that the radiogenic Hf in zircons from the NDZ metadiorites was produced after zircon crystallization and that the measured Lu-Hf isotopic values are credible and can be used to calculate the initial Hf isotopic composition (Wu et al., 2007a). Model ages were calculated based on parameters including a decay constant of 1.867×10^{-11} for ^{176}Lu (Griffin et al., 2000), 0.282772 and 0.0332 for the $^{176}Hf/^{177}Hf$ and $^{176}Lu/^{177}Hf$ ratios of the chondrite (Blichert-Toft and Albarède, 1997), and 0.28325 and 0.0384 for the present day $^{176}Hf/^{177}Hf$ and $^{176}Lu/^{177}Hf$ values of the depleted mantle (Griffin et al., 2000), respectively. Approximate zircon crystallization ages (130 Ma for igneous zircons and 125 Ma for rims) were inferred to calculate the initial isotopic ratios and the two-stage depleted mantle model ages. Seventeen analytical spots on ten zircon cores and seven zircon rims of sample 1310YZH5 yielded $^{176}Hf/^{177}Hf$ ratios of 0.281917–0.282016, with calculated εHf(t) values and T_{DM2} ages ranging from −27.6 to −24.0 and from 2692 to 2911 Ma (Figs. 10), respectively. Analysis on samples 1505LNA1 and 1505XPG1-1 gave coincident results with sample 1310YZH5, with measured $^{176}Hf/^{177}Hf$ ratios of 0.281951–0.282079 (seven zircon cores and five rims) and 0.281859–0.282018 (12 zircon cores), respectively. The corresponding εHf(t) values of the two samples range from −24.8 to −22.0 and from −29.5 to −23.9, respectively, while the calculated T_{DM2} ages vary from 2549 to 2832 Ma and from 2683 to 3084 Ma (Fig. 10), respectively.

Whole-Rock Rb-Sr, Sm-Nd, and Pb Isotopes

Based on zircon U-Pb SHRIMP dating, the initial Sr, Nd, and Pb isotopic ratios of eight metadiorite samples were calculated back to 130 Ma (Table S6; see footnote 1), which is interpreted as the approximate formation or crystallization time of the NDZ metadiorites. The metadiorites have relatively homogeneous initial $^{87}Sr/^{86}Sr$ ratios varying from 0.707582 to 0.708099, while the calculated $\varepsilon_{Nd}(t = 130\ Ma)$ values are negative and variable ranging from −15.3 to −20.4 (Fig. 11A). Neither Sr nor Nd isotopic ratios show notable correlations with whole-rock SiO_2 or K_2O contents (Figs. 11B–11E). In addition, all the samples exhibit consistent Pb isotopic characters, with initial $^{206}Pb/^{204}Pb$, $^{207}Pb/^{204}Pb$, and $^{208}Pb/^{204}Pb$ ratios ranging between 16.0978 and 16.8452, 15.3167–15.4544, and 37.1778–37.8397, respectively (Figs. 11F and 11G).

DISCUSSION

Timing of Emplacement and Metamorphism of the Metadiorites

The studied metadiorites from the NDZ occur within granitic orthogneisses and/or migmatites and show clear gneissic structure and mineral stretching lineations (Fig. 2). Despite the metadiorites occasionally showing similar chemical features with their country rocks, especially the melanosomes of the migmatites (Wang et al., 2007; Yang et al., 2020), crucial evidence obtained from whole-rock elemental and zircon geochronological analyses suggests that they have different genesis and evolutional processes. The metadiorites are coarse-grained with minerals generally larger than those of the country rocks, suggesting that they experienced longer crystallization time spans at lower cooling rates. Besides, the metadiorites, similar to the migmatites, are considered to have undergone partial melting based on the microstructures (Figs. 3H, 3J, and 3K). However, the NDZ migmatites are primarily a mixing of melanosomes (residuum) and related leucosomes (melts), and their protoliths generally were granitoids more felsic than the melanosomes (Yang et al., 2020). In contrast, no distinct evidence of representative melt phases, such as leucosomes and leucocratic veins that occurred during anatexis and migmatization, was found in the metadiorites. Moreover, the surrounding rocks generally retain multiple zircon age-records related to the Triassic subduction-exhumation and to the Neoproterozoic precursors (Liu et al., 2007b, 2011a; Yang et al., 2020), whereas there is no evidence

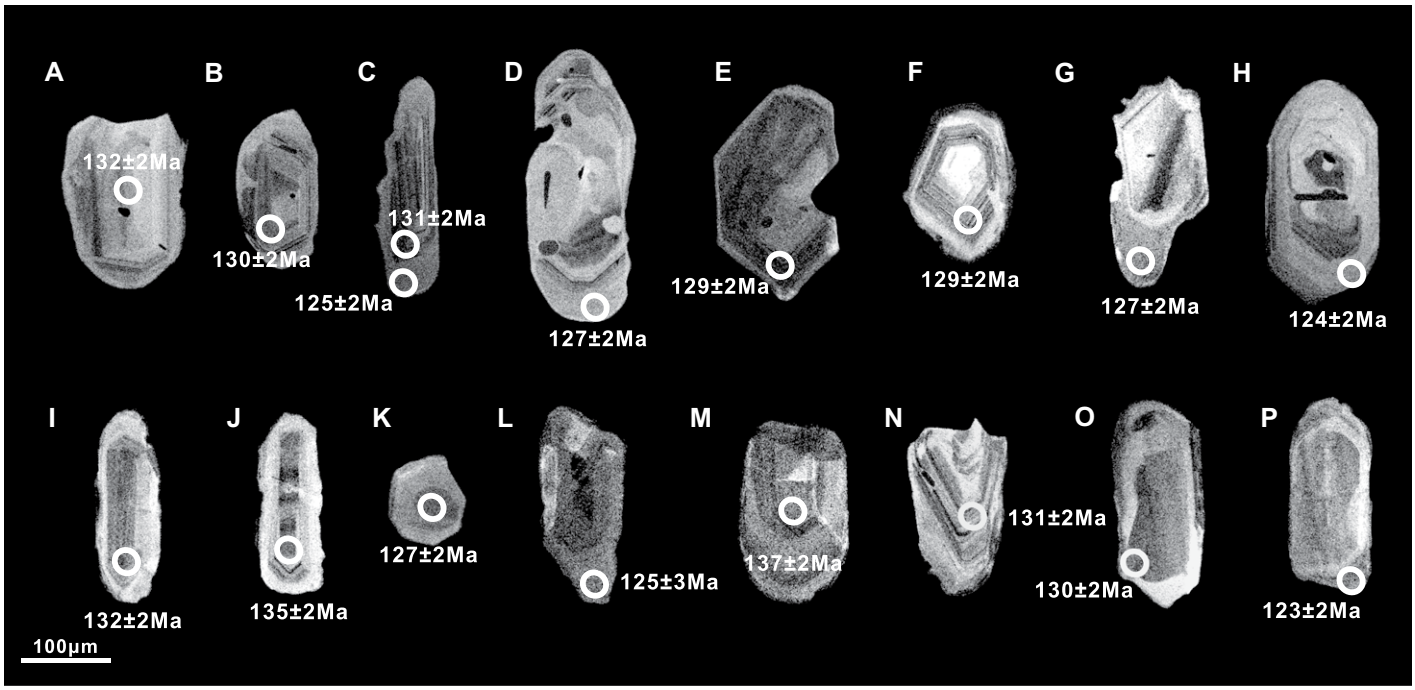

Figure 8. Cathodoluminescence images of representative zircons from metadiorites in the North Dabie complex zone in central China. (A–D) Zircons in sample 1310YZH5; (E–H) zircons in sample 1505LNA1; (I–L) zircons in sample 1505MSH2; (M–P) zircons in sample 1505XPG1-1. All samples were analyzed with a sensitive high-resolution ion microprobe with a 24-μm beam. The white open circles are analysis spots with available $^{206}Pb/^{238}U$ ages.

of pre-Cretaceous events recorded in metadiorite zircon (Figs. 8 and 9).

On the other hand, the metadiorites underwent subsequent metamorphic overprinting and structural reworking, producing pervasive foliation, abundant Kfs porphyroblasts (Fig. 2), green amphiboles and related plagioclases (Figs. 3C and 3D), and homogeneous overgrowth rims on zircons (Fig. 8). Some zircon cores and rims in the metadiorite occasionally have similar U-Pb age records within error; however, typical core-rim textures of zircon CL images with different trace element features, such as Th/U ratios and U contents, allow to clearly distinguish the two tectono-thermal events (Belousova et al., 2002; Corfu et al., 2003). Oscillatory zoned cores display typical characters of magmatic zircons with high Th/U ratios (Rubatto and Gebauer, 2000; Möller et al., 2003). Four samples of the metadiorites yield coincident concordant mean $^{206}Pb/^{238}U$ ages of 129 ± 1 Ma, 131 ± 1 Ma, 133 ± 1 Ma, and 132 ± 2 Ma, respectively, indicating that the metadiorite protolith crystallized from magma at ca. 130 Ma (Fig. 9).

Some zircon cores are well preserved and idiomorphic while others are truncated or corroded and display embay structures (Fig. 8), indicating that they suffered high-T thermal events after crystallization (Keay et al., 2001). In comparison to the igneous zircon cores, zircon rims generally have lower U and Th contents with relatively lower Th/U ratios (Table S3), and exhibit no-zonation structure in CL images (Figs. 8C, 8D, 8G, 8H, 8L, and 8P). Moreover, zircon overgrowth rims generally share coincident Hf isotopic characters with the cores (Fig. 10), suggesting a genetic relationship between them rather than an external genesis. Zircon rims from four metadiorite samples gave similar concordant $^{206}Pb/^{238}U$ ages of ca. 125 Ma with weighted mean ages of 127 ± 2 Ma, 124 ± 2 Ma, 126 ± 3 Ma, and 122 ± 2 Ma, respectively (Fig. 9), in agreement with the timing of migmatization in the region (Liu et al., 2007b; Yang et al., 2020). Since metamorphic zircons have relatively low Th/U ratios (Rubatto and Gebauer, 2000; Möller et al., 2003), and the zircon rims display slightly lower REE contents (Geisler et al., 2003; Hoskin, 2005), we infer the low-Th/U homogeneous rims were metamorphic overgrowth rims crystallized in anatectic melts produced by a high-temperature (HT) event. Moreover, zircon rims exhibit lower total REE contents and steeper HREE patterns with depleted MREE (Fig. 7C), suggesting amphibole crystallization (Tiepolo et al., 2007; Hu et al., 2016) related to HT amphibolite-facies metamorphism. In this regard, they may provide a constraint on the coeval nature of crustal melting and high-T metamorphism at ca. 125 Ma. Various degrees of zircon core corrosion among four samples (Fig. 8) may suggest that the peak-T and duration of this subsequent HT overprinting might have been variable in different localities.

Origin of K-feldspar Porphyroblasts

Large augen K-feldspar porphyroblasts (Fig. 2) are generally wrapped by the foliation of the metadiorites in the NDZ. The porphyroblasts are variable in size ranging from 0.1 to 1.5 cm (Fig. 2) in different samples and exhibit no pronounced compositional zoning (Fig. 3J). Inclusions in the Kfs porphyroblasts can be divided into two subgroups: primary mineral inclusions consisting of biotite (Bt), plagioclase (Pl), and quartz (Qz) (Fig. 3E) and secondary Pl + Qz myrmekite inclusions (Fig. 3J).

As mentioned above, the Kfs also occurs in other textural domains, such as in myrmekites or coronas around Kfs porphyroblasts, in the matrix, and as inclusions in plagioclase or amphibole (Figs. 3G–3I, 3K, and 3L). However, different types of Kfs (Fig. 4B) show variable chemical compositions. The Kfs porphyroblasts ($An_{0–1}Ab_{14–19}Or_{80–86}$) display the lowest K contents and the highest Na contents among all types of Kfs, while Kfs inclusions ($An_{0–1}Ab_{10–11}Or_{89–90}$) and Kfs grains ($An_{0–1}Ab_{1–8}Or_{92–99}$) in the matrix

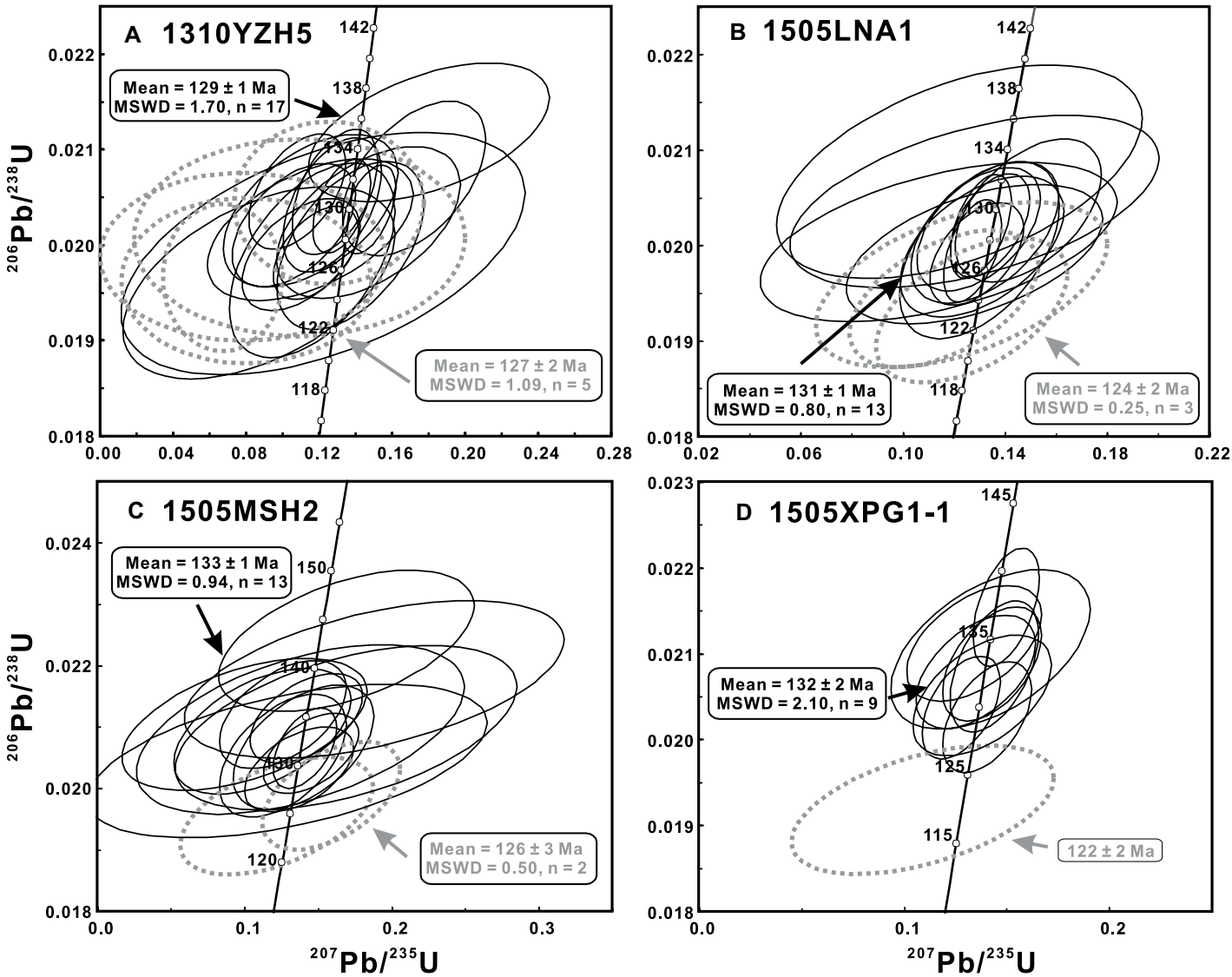

Figure 9. Zircon sensitive high-resolution ion microprobe U-Pb dating of metadiorites in the North Dabie complex zone in central China. (A) Sample 1310YZH5; (B) sample 1505LNA1; (C) sample 1505MSH2; and (D) sample 1505XPG1-1. Size of uncertainty envelopes is 2σ. Different colors of curves indicate that they were dated from different zircon domains (black for igneous cores and gray for rims). MSWD—mean square weighted deviation.

have distinguishable lower Na contents. Primary mineral inclusions of biotite and plagioclase in the Kfs porphyroblasts are generally euhedral (Fig. 3J) and aligned along the lattice face and have consistent chemical compositions with the same minerals in the matrix (Fig. 4C), suggesting the matrix was already crystallized before Kfs porphyroblasts growth (Dyck et al., 2020). This inference is also supported by the contact relationship between the porphyroblasts and the adjacent minerals (Figs. 3J and 3K); Kfs porphyroblasts and plagioclase in direct contact generally have regular boundaries which differs from the Kfs and plagioclase boundaries in the matrix, indicating that the crystallization of Kfs in the matrix and of Kfs porphyroblasts was discontinuous.

Although the Kfs porphyroblasts vary in both size and quantity among different samples, no distinct correlation between whole-rock K_2O and SiO_2 contents or Sr-Nd isotopic ratios were observed (Figs. 11B–11E), precluding the possibility of an external potassium source, such as K-rich fluids or melts injection. The porphyroblasts likely crystallized from anatectic melts after the metadiorite remelted or formed by mineral decomposition and grain coarsening under sub-solidus conditions. Microtextural evidence such as thin Kfs films between biotites and plagioclases (Fig. 3H) and embayment structures, could suggest that the metadiorites may have experienced partial melting, providing the possibility for coarse-grained Kfs crystallization in the presence of a liquid phase (Dell'Angelo and Tullis, 1988; Evans et al., 2001). However, evidence of high-degree partial melting such as leucocratic veins or mineral aggregation after diorite formation was not observed at the outcrop scale (Fig. 2). Hence, if the metadiorite experienced anatexis, the volume of the anatectic melt would be too small to provide the space and convection conditions for Kfs porphyroblast formation. Additionally, monzodioritic magmas are generally Kfs-undersaturated, and would not form such high modal proportions of Kfs as

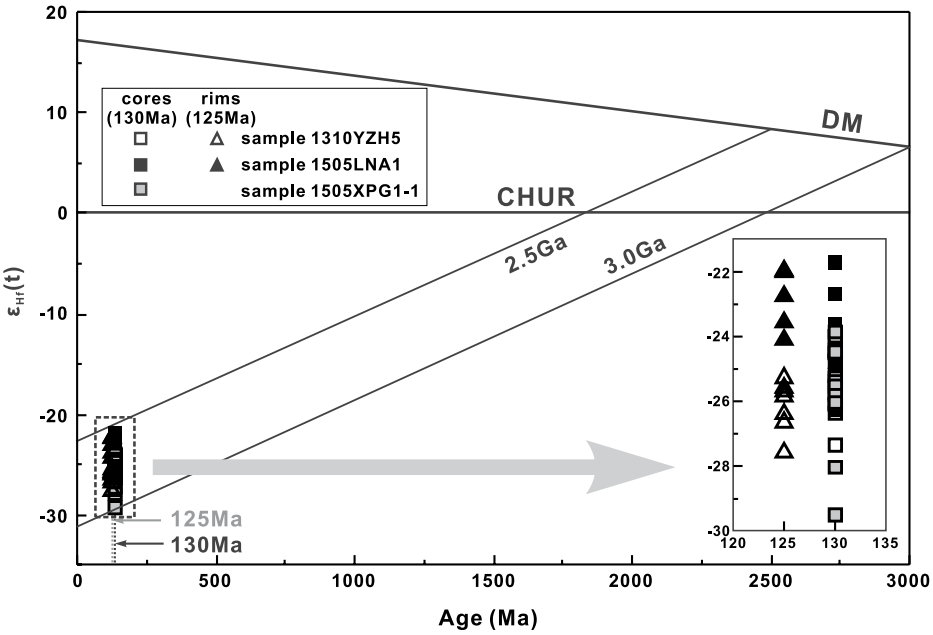

Figure 10. Zircon $^{206}Pb/^{238}U$ ages versus $\varepsilon_{Hf}(t)$ values of the metadiorites in the North Dabie complex zone in central China. CHUR—chondritic uniform reservoir; DM—depleted mantle.

found in the NDZ metadiorites. Therefore, protolith remelting is unlikely to be the predominant mechanism of formation for the Kfs porphyroblasts in the metadiorites.

A possible origin of potassium could be the breakdown of K-rich minerals, such as biotite (Büsch et al., 1974; Cruciani et al., 2008; Álvarez-Valero and Kriegsman, 2010). All the samples in this study contain large amount of biotites which occur as euhedral to anhedral grains in matrix and inclusions in both Kfs porphyroblasts and other minerals. Breakdown of biotite provides a potential reservoir of potassium necessary for porphyroblasts crystallization. This speculation is also supported by the primary inclusions of biotite and plagioclase distributed along the lattice faces in the Kfs porphyroblasts (Fig. 3E). The porphyroblasts also contain clusters of fine-grained quartz inclusions, while inclusions in the rims are generally more coarse-grained than in the cores, suggestive of metamorphic genesis (Dyck et al., 2020).

The Kfs porphyroblasts in the NDZ metadiorites generally lack syntectonic multiphase solid inclusions, resulting in difficulty calculating the precise temperature and pressure of crystallization. However, since Kfs porphyroblasts were crystallized after the formation of the matrix as discussed above, we assume the metadiorite didn't experience pressure increase after their formation at ca. 130 Ma, as no such geological events were reported in this region. Therefore, the Kfs porphyroblasts were crystallized at pressures lower than the pressure values constrained using minerals in the matrix. Al-in-hornblende barometry applied to rocks with a mineral assemblage of Amp + Pl + Bt + Or + Qz + Ttn + Mag (Ilm) (Schmidt, 1992) can be used to determine the pressure of hornblende crystallization in the matrix of the metadiorite and the amphibole crystallization pressures were calculated to 4.5−5.7 kbar. Therefore, we consider 4.5 kbar, which was estimated with a low-Ti and low-Al^{IV} amphibole rim as the maximum pressure of the Kfs porphyroblasts formation. Under this premise, the temperature of Kfs porphyroblasts crystallization was calculated to be 640–703 °C using two-feldspar geothermometer (Benisek et al., 2010) combining Kfs porphyroblast rims and plagioclase in adjacent myrmekites (Table S7; see footnote 1).

The field occurrence of augen Kfs porphyroblasts wrapped by the foliation of the metadiorites indicates the metadiorite underwent strongly shear deformation (Fig. 2). The Kfs porphyroblasts are generally surrounded by myrmekites of plagioclase, quartz, and Kfs (Figs. 3J–3L), which were related to fluid alteration (Abart et al., 2014; Touret and Huizenga, 2012; Newton and Manning, 2000), providing evidence of ductile shear deformation (Menegon et al., 2006).

Genesis of Metadiorites

As depicted in Figures 7A and 7B, the metadiorites in the NDZ are enriched in water-soluble elements such as LREEs and LILEs (e.g., Becker et al., 2000; John et al., 2004), and depleted in HFSEs, exhibiting arc-like patterns of trace element distribution. Whole-rock Sr, Nd, and Pb isotopic ratios of metadiorites show no correlation with K_2O and SiO_2 contents (Figs. 11B–11E), suggesting that the dissolution of accessory minerals such as apatite and monazite are negligible toward the Sr-Nd-Pb isotopic constitution and there were no injections of external melts or fluids after the formation of diorites. All samples in this study exhibit homogeneous and low initial $^{87}Sr/^{86}Sr$ ratios (range of 0.707582–0.708099 calculated to 130 Ma) and negative $\varepsilon_{Nd}(130\ Ma)$ values (−15.3 to −20.4), with relatively low initial Pb isotopic ratios (Figs. 11F and 11G). However, Nd model ages of the NDZ metadiorites range between 2.2 and 2.6 Ga as outlined in Table S5, which are younger than the zircon Hf model ages with values of 2.5–3.1 Ga (Fig. 10). Hence, zircon Hf model ages are quite reasonable for the age of source rocks (Kemp et al., 2006; Nebel et al., 2007), in consideration of zircon Hf isotopic stability and of whole-rock Sm-Nd isotopic variability that resulted from Sm-Nd differentiation during anatexis (Patchett et al., 1984). The εHf(t) values of zircon igneous cores (calculated to t = 130 Ma) and the metamorphic overgrowth rims (calculated to t = 125 Ma) in the metadiorites are almost consistent and highly negative, ranging from −29.5 to −21.7 and from −27.6 to −22.0, respectively. The arc-like whole-rock trace element pattern, highly negative zircon εHf(t) and whole-rock εNd(t) values, as well as the Archean Hf model ages of the NDZ metadiorites mentioned above, demonstrate that an ancient continental crust played an important role in their petrogenesis (Fan et al., 2004; Jahn et al., 1999). In addition, their Zr and Hf contents exhibit no obvious depletion, while Ba contents display significant positive anomalies relative to Rb and Th. This suggests a lower continental crust genesis (Rudnick and Gao, 2003) in response to a common source from the Triassic subducted Neoproterozoic lower-crustal rocks (Liu et al., 2007a; Yang et al., 2020) (Fig. 7B).

The studied metadiorites display low initial $^{87}Sr/^{86}Sr$, $^{143}Nd/^{144}Nd$, and Pb isotopic ratios (Figs. 11A, 11F, and 11G), similar to those of UHP metamorphic rocks in the NDZ such as eclogite and granitic orthogneiss likely suggesting a genetic relationship in the source region between the metadiorites and the UHP metamorphic rocks in the NDZ. However, the exposed Dabie granitic orthogneisses and NDZ eclogites have dominantly Paleoproterozoic zircon Hf model ages (Zhao et al., 2008; Gu, 2012), which are younger than those of the metadiorites. Therefore, the overall features of the metadiorites

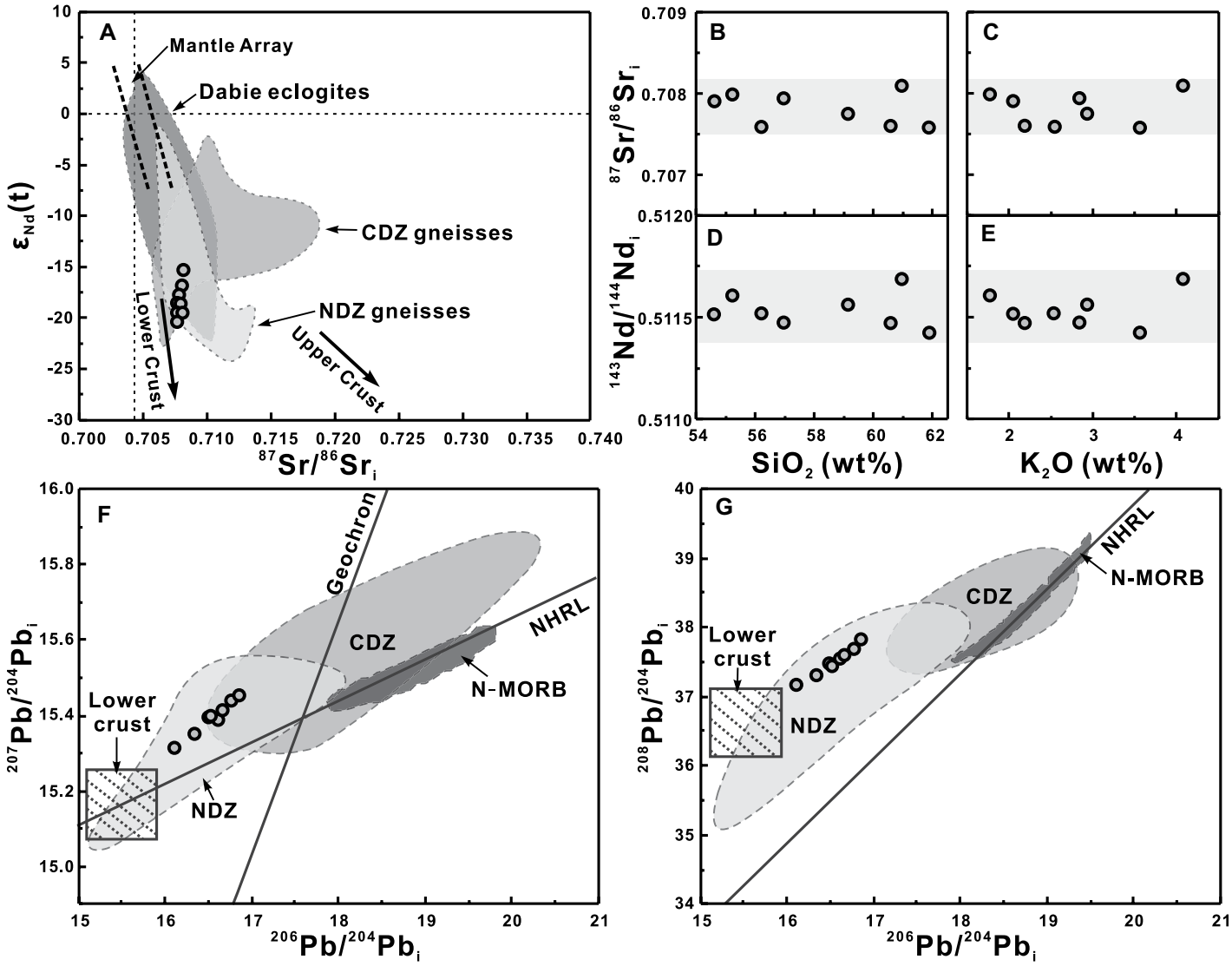

Figure 11. Whole-rock Sr-Nd-Pb isotopic scatter diagrams of metadiorites in the North Dabie complex zone (NDZ) in central China. (A) $^{87}Sr/^{86}Sr_i$ versus ε_{Nd}(130 Ma) diagram; (B) SiO_2 (wt%) versus $^{87}Sr/^{86}Sr_i$ diagram; (C) K_2O (wt%) versus $^{87}Sr/^{86}Sr_i$ diagram; (D) SiO_2 versus $^{143}Nd/^{144}Nd_i$ diagram; (E) K_2O (wt%) versus $^{143}Nd/^{144}Nd_i$ diagram; (F) initial $^{206}Pb/^{204}Pb$ versus $^{207}Pb/^{204}Pb$ diagram; (G) initial $^{206}Pb/^{204}Pb$ versus $^{208}Pb/^{204}Pb$ diagram. Representative Sr-Nd isotopic data for the Central Dabie ultrahigh-pressure metamorphic zone (CDZ) gneisses, NDZ gneisses, and Dabie eclogites are from Liu et al. (2020). The arrows point to lower and upper crust, respectively. The light gray and gray fields in (F and G) represent data for the ultrahigh-pressure orthogneisses and eclogites from the NDZ and CDZ, respectively (modified from Yang et al., 2020). N-MORB—normal mid-ocean ridge basalt; NHRL—northern hemisphere reference line.

cannot be explained by partial melting of only the mafic UHP rocks, and their genesis seems to require the involvement of unexposed, more ancient, Archean-sourced materials.

The metadiorites generally display high Sr contents (814–1242 ppm), high $Mg^{\#}$ values (44.2–50.3), and relatively high SiO_2 contents (55.21–61.87 wt%). Several samples with low Y contents and high Sr/Y ratios display high-Mg adakitic alike geochemical features (Fig. 6) which were probably produced by melting of hydrous peridotite (e.g., Stern and Hanson, 1991). The distinctive geochemical characteristics of metadiorite could be caused by two possible mechanisms, considering the petrotectonic setting of the Dabie orogen: continental crustal contamination and crust-mantle interaction (Zhao et al., 2011). Composition of magma Sr-Nd isotopes may be modified by crustal contamination during upward migration or uplift. However, the linear Sr-Nd isotopic ratios show no correlation with whole-rock SiO_2 contents (Figs. 11B and 11D) of metadiorite, suggesting that source heterogeneity should be the dominant factor instead of continental crustal contamination coupled with assimilation-fractionation crystallization during magma migration. On the other hand, high-Mg silicic melts could be produced by SiO_2-rich melt assimilating peridotite with melt/rock ratios over 2:1 (Rapp et al., 1999) without SiO_2 content decreasing significantly (Huang et al., 2008). Since the diorites exhibit the "lower continental crust"-like features such as Sr-Nd-Pb compositions, trace element patterns combined with high MgO, Cr, and Ni contents, and higher Sr/Y ratios, they were more likely derived from partial melting of a lower crustal source, combined with minor mantle peridotite assimilation.

The amphibole formation temperatures were calculated to 4.5–5.7 kbar by Al-in-hornblende barometry (Schmidt, 1992). Amp1 are generally brown and display higher Al and Ti contents with higher calculated crystallization pressures of 5.4–5.7 kbar. Meanwhile, the green low-Al and low-Ti Amp2 were formed under lower pressures of 4.5–5.3 kbar. Combining this method with the amphibole-plagioclase thermometer (Holland and Blundy, 1994), the formation temperature conditions of Amp1 and Amp 2 in the matrix should be 750–768 °C and 712–736 °C calculated with amphibole grains and co-existing plagioclase inclusions, respectively (Table S7). Al contents in green amphiboles decrease from core to rim, suggesting that amphiboles grew during upward migration under reducing pressure conditions. Therefore, it is further inferred that the NDZ metadiorites were derived from UHP metamorphic lower-crustal rocks in the subducted NDZ terrane in the Cretaceous.

IMPLICATIONS IN THE FRAMEWORK OF MOUNTAIN-ROOT COLLAPSE

The evolution of collisional orogens generally comprises a period of crustal thickening followed by extension and thinning of the previously thickened crust involved in mountain-root collapse (Dewey, 1988; Vissers et al., 1995; Brown, 2001; Rey et al., 2001; Vanderhaeghe and Teyssier, 2001). There is, however, clear evidence for melting during collapse in the late stages of the evolution of many orogens formed by collisional processes, generally linked to lithosphere delamination or slab detachment (von Blanckenburg and Davies, 1995; Davies and von Blanckenburg, 1995; Brown, 2001; Liu and Zhang, 2020; and references therein). In the Dabie orogen, the formation of migmatites, as well as of the Early Cretaceous granites, gabbros, and (meta)diorites may be related to the extension and thinning of thickened crust formed during the Mesozoic continental collision. The Dabie orogen is a typical "complete" orogen (Leech, 2001) that experienced an evolution cycle that progresses from subduction-collision and uplift, to metamorphism and delamination of the crustal root, to final tectonic collapse. Furthermore, the NDZ terrane suffered large-scale partial melting and migmatization in the Early Cretaceous, leading to the production of a variety of migmatites with different leucosomes (Liu et al., 2007b; Wu et al., 2007b; Wang et al., 2013; Xu and Zhang, 2017; Yang et al., 2020) and magmatic intrusions (Jahn et al., 1999; Li et al., 1999; Chen et al., 2002; Wang et al., 2007; Zhao et al., 2005, 2007). All of this evidence strongly suggests that the transition of the tectonic regime from compression to extension related to mountain-root collapse occurred at ca. 130 Ma (Ma et al., 2003; Xu et al., 2007; He et al., 2011; Li et al., 2013). The studied (meta) diorites are rarely exposed but bring new insights to understanding the evolution of the Dabie orogen during post-collisional mountain-root collapse and other orogens in general.

As previously mentioned, the metadiorites' precursors were derived from the Triassic UHP eclogites with the addition of minor amounts of mantle-derived materials during the Cretaceous post-collisional event in the Dabie orogen. The UHP lower crustal metamorphic rocks of the NDZ underwent partial melting after detachment and sank into the asthenospheric mantle in the Cretaceous, accompanied by fluid injection and heating. The SiO_2-rich melt produced from this melting assimilated mantle rocks, such as peridotite, while migrating upwards to shallow crustal levels, intruding into gneisses and migmatites at ca. 130 Ma. After magma crystallization, subsequent HT metamorphism, deformation, and potassic alteration, the (meta) diorites were emplaced in the NDZ together with various country rocks by collisional orogenesis and erosion. We propose a new tectonic scenario for the Dabie orogen from subduction to exhumation and post-collisional collapse, from the Late Triassic to Early Cretaceous as illustrated in Figure 12.

The northward subduction of the SCB beneath the NCB during the Late Triassic (Xu et al., 1992; Li et al., 1993; Jahn et al., 1999;

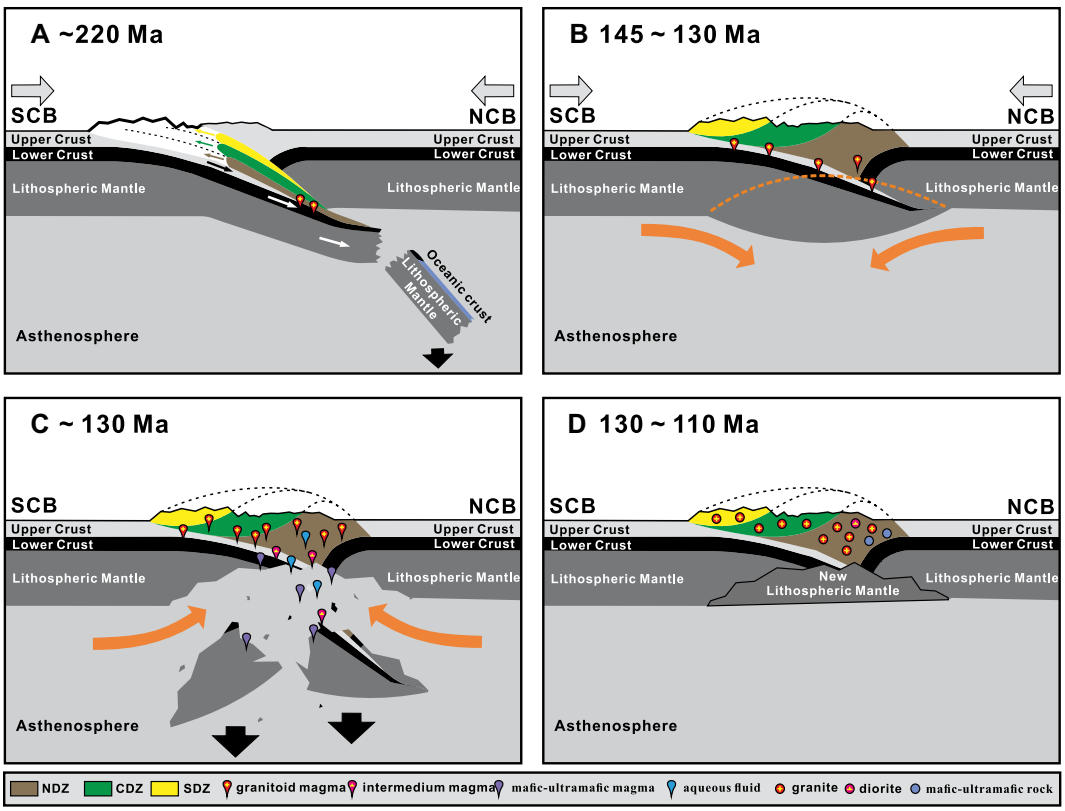

Figure 12. Tectonic cartoons showing continent-continent collision, mountain root collapse, and post-collisional magmatism in the Dabie orogen in central China. (A) Subduction of the South China Block (SCB) beneath the North China Block (NCB) in the Triassic. (B) Overthickened lower crust and lithospheric mantle resulting from continuous convergence of NCB and SCB, led to gravitational instability in the Early Cretaceous. (C) Mountain-root collapsed and sunk to the asthenosphere, causing asthenosphere upwelling and extensive magmatic events at ca. 130 Ma. (D) Asthenosphere replaced the detached lithospheric mantle and reformed the new lithospheric mantle after cooling. NDZ—North Dabie complex zone; CDZ—Central Dabie ultrahigh-pressure metamorphic zone; SDZ—South Dabie low-temperature eclogite zone.

Liu et al., 2007b, 2011a, 2011b) caused UHP metamorphism, slab breakoff, and initial uplift from mantle-depths to middle-upper crustal levels (Fig. 12A). However, after the deeply subducted slab broke off and foundered into the asthenosphere, the convergence between the NCB and the SCB persisted as proposed by Liu et al. (2007b), leading to thickening of the lithosphere and the construction of the Dabie orogen (Fig. 12B) through the Early Cretaceous (Li et al., 1999; Yang et al., 2020). During this stage, mineral assemblages were transformed from the original basaltic/gabbroic paragenesis to granulite/eclogite/garnet amphibolite assemblages in the lower crust (Wolf and Wyllie, 1994; Rapp and Watson, 1995), with consequent density increase and gravitative instability of the over-thickened lithosphere (Lustrino, 2005). The cold thickened lithosphere protruded downward into the hot asthenospheric mantle and produced convection from the upper-mantle to the mountain-root as a result of temperature differences. As a consequence, the unstable lower crust and the underlying lithospheric mantle detached and sank into the asthenospheric mantle (Fig. 12C) at ca. 130 Ma, leading to mountain-root collapse. In the meantime, the lower-crustal rocks underwent partial melting and produced melts with adakitic affinity (Springer and Seck, 1997; Defant and Kepezhinskas, 2001), which were largely emplaced as felsic granitoid intrusions. In addition, anatexis and mixing of lithospheric mantle and mafic lower-crustal rocks produced the mafic-ultramafic rocks, such as gabbro and pyroxenite (Jahn et al., 1999; Li et al., 1999; Zhao et al., 2011), as well as the studied diorites. After mountain-root collapse, new asthenospheric mantle replaced the delaminated lithospheric mantle and lower crust (Lustrino, 2005). After subsequent exhumation, doming, décollement, and erosion, the NDZ UHP rocks and migmatites were tectonically merged with abundant post-collisional igneous rocks including granites, diorites, and mafic-ultramafic lithologies; the whole tectonic package was subjected to near-coeval metamorphism and conspicuous deformation (Fig. 12D). This tectonic scenario is also supported by extensive anatexis and related thermal metamorphism preserved in the eclogites, granitic gneisses, and migmatites of the NDZ during the Cretaceous as previously documented by Liu et al. (2007b), Wu et al. (2007b), Wang et al. (2013), Xu and Zhang (2017), Deng et al. (2019), and Yang et al. (2020).

CONCLUSIONS

The post-collisional metadiorites in the Dabie orogen have typical continental signatures in regards to elemental and isotopic geochemistry; these signatures coincide with those of the NDZ UHP metamorphic rocks. They are characterized by intermedium SiO_2 contents and $Mg^{\#}$ values, highly negative $\varepsilon Nd(t)$ and $\varepsilon Hf(t)$ values, and late Archean Hf two-stage model ages, suggesting a mixing of dominant Triassic subducted lower-crustal UHP metamorphic mafic rocks and minor mantle-derived materials. In the Early Cretaceous, over-thickened lower crust and lithosphere produced by the convergence of the North China and South China blocks detached and foundered downward to the asthenosphere at ca. 130 Ma. This foundering resulted in the anatexis and mixing of lower crust- and mantle-derived materials, producing a series of igneous rocks such as diorites during mountain-root collapse. The diorites formed at ca. 130 Ma, and subsequently experienced HT metamorphism at ca. 125 Ma. In addition, the formation of the distinctive K-feldspar porphyroblasts is likely a result of crystallization derived from biotite breakdown at $T = 640–703$ °C and $P < 4.5$ kbar and coarsening related to shear deformation.

ACKNOWLEDGMENTS

This study was supported by funds from the National Natural Science Foundation of China (41273036 and 42072059) and the National Basic Research Program of China (2015CB856104). We thank B. Song and C. Yang for help with sensitive high-resolution ion microprobe U-Pb dating on zircon, Z.-H. Hou for trace-element analysis on zircon, P. Sun and T. Yang for zircon Hf isotope analysis, F.-K. Chen for the Sr-Nd-Pb isotopic analysis, and Y.-H. Shi and J. Wang for the electron microprobe analysis. We are grateful to Rob Strachan and Jeff Hannon for editorial handling and comments, and Antonio M. Álvarez-Valero, Ellen Alexander, and an anonymous reviewer for their many constructive reviews and suggestions, which greatly improved the presentation.

REFERENCES CITED

Abart, R., Heuser, D., and Habler, G., 2014, Mechanism of myrmekites formation: Case study from the Weinsberg granite, Modanubian zone, Upper Austria: Contributions to Mineralogy and Petrology, v. 168, no. 1074, https://doi.org/10.1007/s00410-014-1074-7.

Álvarez-Valero, A.M., and Kriegsman, L.M., 2010, Chemical, petrological and mass balance constraints on the textural evolution of pelitic enclaves: Lithos, v. 116, p. 300–309, https://doi.org/10.1016/j.lithos.2009.09.009.

Atherton, M.P., and Petford, N., 1993, Generation of sodium-rich magmas from newly underplated basaltic crust: Nature, v. 362, p. 144–146, https://doi.org/10.1038/362144a0.

Baird, D.J., Nelson, K.D., Knapp, J.H., Walters, J.J., and Brown, L.D., 1996, Crustal structure and evolution of the Trans-Hudson orogen: Results from seismic reflection profiling: Tectonics, v. 15, p. 416–426, https://doi.org/10.1029/95TC02425.

Becker, H., Jochum, K.P., and Carlson, R.W., 2000, Trace element fractionation during dehydration of eclogites from high-pressure terranes and the implications for element fluxes in subduction zones: Chemical Geology, v. 163, p. 65–99, https://doi.org/10.1016/S0009-2541(99)00071-6.

Belousova, E., Griffin, W.L., O'Reilly, S.Y., and Fisher, N.L., 2002, Igneous zircon: Trace element composition as an indicator of source rock type: Contributions to Mineralogy and Petrology, v. 143, no. 5, p. 602–622, https://doi.org/10.1007/s00410-002-0364-7.

Benisek, A., Dachs, E., and Kroll, H., 2010, A ternary feldspar-mixing model based on calorimetric data: Development and application: Contributions to Mineralogy and Petrology, v. 160, p. 327–337, https://doi.org/10.1007/s00410-009-0480-8.

Berzin, R., Oncken, O., Knapp, J.H., Perez-Estaún, A., Hismatulin, T., Yunosov, N., and Lipilin, A., 1996, Orogenic evolution of the Ural Mountains: Results from an integrated seismic experiment: Science, v. 274, p. 220–221, https://doi.org/10.1126/science.274.5285.220.

Black, L.P., Kamo, S.L., Allen, C.M., Aleinikoff, J.N., Davis, D.W., Korsch, R.J., and Foudoulis, C., 2003, TEMORA 1: A new zircon standard for Phanerozoic U-Pb geochronology: Chemical Geology, v. 200, no. 1, p. 155–170, https://doi.org/10.1016/S0009-2541(03)00165-7.

Blichert-Toft, J., and Albarède, F., 1997, The Lu-Hf isotope geochemistry of chondrites and the evolution of the mantle-crust system: Earth and Planetary Science Letters, v. 148, p. 243–258, https://doi.org/10.1016/S0012-821X(97)00040-X.

Boynton, W.V., 1984, Geochemistry of the rare earth elements: Meteorite study, *in* Henderson, P., ed., Rare Earth Element Geochemistry: Amsterdam, Netherlands, Elsevier, p. 63–114, https://doi.org/10.1016/B978-0-444-42148-7.50008-3.

Brown, M., 2001, Orogeny, migmatites and leucogranites: A review: Proceedings of the Indiana Academy of Sciences, v. 110, p. 313–336, https://doi.org/10.1007/BF02702898.

Bryant, D.L., Ayers, J.C., Gao, S., Miller, C.F., and Zhang, H., 2004, Geochemical, age, and isotopic constraints on the location of the Sino-Korean/Yangtze Suture and evolution of the Northern Dabie Complex, east central China: Geological Society of America Bulletin, v. 116, p. 698–717, https://doi.org/10.1130/B25302.2.

Büsch, W., Schenider, G., and Mehnert, K., 1974, Initial melting at grain boundaries. Part II: Melting in rocks of granodioritic, quartzdioritic and tonalitic composition: Neues Jahrbuch für Mineralogie Monatshefte, v. 8, p. 345–370.

Carbonell, R., Perez-EstaÚn, A., Gallart, J., Diaz, J., Kashubin, S., Mechie, J., Stadtlander, R., Schulze, A., Knapp, J.H., and Morozov, A., 1996, Crustal root beneath the Urals: Wide-angle seismic evidence: Science, v. 274, p. 222–224, https://doi.org/10.1126/science.274.5285.222.

Chen, B., Jahn, B.M., and Wei, C.J., 2002, Petrogenesis of Mesozoic granitoids in the Dabie UHP complex, Central China: Trace element and Nd-Sr isotope evidence: Lithos, v. 60, p. 67–88, https://doi.org/10.1016/S0024-4937(01)00077-9.

Chen, F., Hegner, E., and Todt, W., 2000, Zircon ages and Nd isotopic and chemical compositions of orthogneisses from the Black Forest, Germany: Evidence for a Cambrian magmatic arc: International Journal of Earth Sciences, v. 88, p. 791–802, https://doi.org/10.1007/s005310050306.

Chen, F., Li, X.H., Wang, X.L., Li, Q.L., and Siebel, W., 2007, Zircon age and Nd-Hf isotopic composition of the Yunnan Tethyan belt, southwestern China: International Journal of Earth Sciences, v. 96, p. 1179–1194, https://doi.org/10.1007/s00531-006-0146-y.

Compston, W., Williams, I.S., and Meyer, C., 1984, U-Pb geochronology of zircons from lunar breccia 73217 using a sensitive high mass-resolution ion microprobe: Journal of Geophysical Research. Solid Earth, v. 89, p. B525–B534, https://doi.org/10.1029/JB089iS02p0B525.

Coney, P.J., and Harms, T.A., 1984, Cordilleran metamorphic core complexes: Cenozoic extensional relics of Mesozoic compression: Geology, v. 12, p. 550–554, https://doi.org/10.1130/0091-7613(1984)12<550:CMCCCE>2.0.CO;2.

Corfu, F., Hanchar, J.M., Hoskin, P.W.O., and Kinny, P., 2003, Atlas of zircon textures: Reviews in Mineralogy and Geochemistry, v. 53, no. 1, p. 469–500, https://doi.org/10.2113/0530469.

Cruciani, G., Franceshelli, M., Jung, S., Puxeddu, M., and Utzeri, D., 2008, Amphibole-bearing migmatites from

the Variscan Belt of NE Sardinia, Italy: Partial melting of mid-Ordovician igneous sources: Lithos, v. 105, no. 3–4, p. 208–224, https://doi.org/10.1016/j.lithos.2008.03.009.

Davies, J.H., and von Blanckenburg, F.V., 1995, Slab breakoff: A model of lithosphere detachment and its test in the magmatism and deformation of collisional orogens: Earth and Planetary Science Letters, v. 129, no. 1–4, p. 85–102, https://doi.org/10.1016/0012-821X(94)00237-S.

Defant, M.J., and Drummond, M.S., 1990, Derivation of some modern arc magmas by melting of young subducted lithosphere: Nature, v. 347, p. 662–665, https://doi.org/10.1038/347662a0.

Defant, M.J., and Kepezhinskas, P., 2001, Evidence suggests slab melting in arc magmas: Eos (Washington, D.C.), v. 82, no. 6, p. 65–68, https://doi.org/10.1029/01EO00038.

Dell'Angelo, L.N., and Tullis, J., 1988, Experimental deformation of partially melted granitic aggregates: Journal of Metamorphic Geology, v. 6, no. 4, p. 495–515, https://doi.org/10.1111/j.1525-1314.1988.tb00436.x.

Deng, L.P., Liu, Y.C., Yang, Y., Groppo, C., Rolfo, F., and Gu, X.F., 2019, Anatexis of high-T eclogites in the Dabie orogen triggered by exhumation and post-orogenic collapse: European Journal of Mineralogy, v. 31, no. 5–6, p. 889–903, https://doi.org/10.1127/ejm/2019/0031-2884.

Dewey, J.F., 1988, Extensional collapse of orogens: Tectonics, v. 7, p. 1123–1139, https://doi.org/10.1029/TC007i006p01123.

Dyck, B., Waters, D.J., St-Onge, M.R., and Searle, M.P., 2020, Muscovite dehydration melting: Reaction mechanisms, microstructures, and implications for anatexis: Journal of Metamorphic Geology, v. 38, no. 1, p. 29–52, https://doi.org/10.1111/jmg.12511.

Evans, B., Renner, J., and Hirth, G., 2001, A few remarks on the kinetics of static grain growth in rocks: International Journal of Earth Sciences, v. 90, no. 1, p. 88–103, https://doi.org/10.1007/s005310000150.

Fan, W.M., Guo, F., Wang, Y.J., and Zhang, M., 2004, Late Mesozoic volcanism in the northern Huaiyang tectonomagmatic belt, central China: Partial melts from a lithospheric mantle with subducted continental crust relicts beneath the Dabie Orogen?: Chemical Geology, v. 209, no. 1–2, p. 27–48, https://doi.org/10.1016/j.chemgeo.2004.04.020.

Gao, S., Jin, Z.M., and Jin, S.Y., 1998, Seismic velocity structure and composition of continental crust in the Dabie-Sulu area: Continental Dynamics, v. 3, p. 108–112.

Gao, S., Rudnick, R., Yuan, H.L., Liu, X.M., Liu, Y.S., Xu, W.L., Ling, W.L., Ayers, J., Wang, X.C., and Wang, Q.H., 2004, Recycling lower continental crust in the North China craton: Nature, v. 432, p. 892–897, https://doi.org/10.1038/nature03162.

Garzanti, E., Radeff, G., and Malusà, M.G., 2018, Slab breakoff: A critical appraisal of a geological theory as applied in space and time: Earth-Science Reviews, v. 177, p. 303–319, https://doi.org/10.1016/j.earscirev.2017.11.012.

Geisler, T., Rashwan, A.A., Rahn, M.K.W., Poller, U., Zwingmann, H., Pidgeon, R.T., Schleicher, H., and Tomaschek, F., 2003, Low temperature hydrothermal alteration of natural metamict zircons from the Eastern Desert, Egypt: Mineralogical Magazine, v. 67, p. 485–508, https://doi.org/10.1180/0026461036730112.

Griffin, W.L., Pearson, N.J., Belousova, E., Jackson, S.E., van Achterbergh, E., O'Reilly, S.Y., and Shee, S.R., 2000, The Hf isotope composition of cratonic mantle: LAM-MC-ICPMS analysis of zircon megacrysts in kimberlites: Geochimica et Cosmochimica Acta, v. 64, no. 1, p. 133–147, https://doi.org/10.1016/S0016-7037(99)00343-9.

Groppo, C., Rolfo, F., Liu, Y.C., Deng, L.P., and Wang, A.D., 2015, P-T evolution of elusive UHP eclogites from the Luotian dome (north Dabie zone, China): How far can the thermodynamic modeling lead us?: Lithos, v. 226, p. 183–200, https://doi.org/10.1016/j.lithos.2014.11.013.

Gu, X.F., 2012, Petrologic geochemistry and isotopic geochronology of the Luotian eclogites from the North Dabie complex zone, central China [Ph.D. thesis]: Hefei, University of Science and Technology of China, 165 p.

Hacker, B.R., Ratschbacher, L., Webb, L.E., Ireland, T.R., Walker, D., and Dong, S., 1998, U/Pb zircon ages constrain the architecture of the ultrahigh-pressure Qinling–Dabie orogen, China: Earth and Planetary Science Letters, v. 161, no. 1–4, p. 215–230, https://doi.org/10.1016/S0012-821X(98)00152-6.

Hacker, B.R., Ratschbacher, L., and Webb, L., 2000, Exhumation of ultrahigh-pressure continental crust in east central China: Late Triassic-Early Jurassic tectonic unroofing: Journal of Geophysical Research. Solid Earth, v. 105, no. B6, p. 13339–13364, https://doi.org/10.1029/2000JB900039.

He, Y.S., Li, S.G., Hoefs, J., Huang, F., Liu, S.A., and Hou, Z.H., 2011, Post-collisional granitoids from the Dabie orogen: New evidence for partial melting of a thickened continental crust: Geochimica et Cosmochimica Acta, v. 75, no. 13, p. 3815–3838, https://doi.org/10.1016/j.gca.2011.04.011.

He, Y.S., Li, S.G., Hoefs, J., and Kleinhanns, I.C., 2013, Sr-Nd-Pb isotopic compositions of Early Cretaceous granitoids from the Dabie orogen: Constraints on the recycled lower continental crust: Lithos, v. 156–159, p. 204–217, https://doi.org/10.1016/j.lithos.2012.10.011.

Holland, T., and Blundy, J., 1994, Non-ideal interactions in calcic amphiboles and their bearing on amphibole-plagioclase thermometry: Contributions to Mineralogy and Petrology, v. 116, p. 433–447, https://doi.org/10.1007/BF00310910.

Hoskin, P.W.O., 2005, Trace-element composition of hydrothermal zircon and the alteration of Hadean zircon from the Jack Hills, Australia: Geochimica et Cosmochimica Acta, v. 69, no. 3, p. 637–648, https://doi.org/10.1016/j.gca.2004.07.006.

Hu, Z.P., Zhang, Y.S., Hu, R., Wang, J., Siebel, W., and Chen, F.K., 2016, Amphibole-bearing migmatite in the North Dabie, eastern China: Water-fluxed melting of the orogenic crust: Journal of Asian Earth Sciences, v. 125, p. 100–116, https://doi.org/10.1016/j.jseaes.2016.05.018.

Huang, F., Li, S.G., Dong, F., Li, Q.L., Chen, F.K., Wang, Y., and Yang, W., 2007, Recycling of deeply subducted continental crust in the Dabie Mountains, central China: Lithos, v. 96, p. 151–169, https://doi.org/10.1016/j.lithos.2006.09.019.

Huang, F., Li, S.G., Dong, F., He, Y.S., and Chen, F.K., 2008, High-Mg adakitic rocks in the Dabie orogen, central China: Implications for foundering mechanism of lower continental crust: Chemical Geology, v. 255, no. 1, p. 1–13, https://doi.org/10.1016/j.chemgeo.2008.02.014.

Jahn, B.M., Wu, F.Y., Lo, C.H., and Tsai, C.H., 1999, Crust–mantle interaction induced by deep subduction of the continental crust: Geochemical and Sr–Nd isotopic evidence from post-collisional mafic–ultramafic intrusions of the northern Dabie complex, central China: Chemical Geology, v. 157, p. 119–146, https://doi.org/10.1016/S0009-2541(98)00197-1.

John, T., Scherer, E.E., Haase, K., and Schenk, V., 2004, Trace element fractionation during fluid-induced eclogitization in a subducting slab: Trace element and Lu–Hf–Sm–Nd isotope systematics: Earth and Planetary Science Letters, v. 227, p. 441–456, https://doi.org/10.1016/j.epsl.2004.09.009.

Kay, R.W., and Kay, S.M., 1991, Creation and destruction of lower continental crust: Geologische Rundschau, v. 80, p. 259–278, https://doi.org/10.1007/BF01829365.

Kay, R.W., and Kay, S.M., 1993, Delamination and delamination magmatism: Tectonophysics, v. 219, no. 1–3, p. 177–189, https://doi.org/10.1016/0040-1951(93)90295-U.

Keay, S., Lister, G., and Buick, I., 2001, The timing of partial melting, Barrovian metamorphism and granite intrusion in the Naxos metamorphic core complex, Cyclades, Aegean Sea, Greece: Tectonophysics, v. 342, no. 3–4, p. 275–312, https://doi.org/10.1016/S0040-1951(01)00168-8.

Kemp, A.I.S., Hawkesworth, C.J., Paterson, B.A., and Kinny, P.D., 2006, Episodic growth of the Gondwana supercontinent from hafnium and oxygen isotopes in zircon: Nature, v. 439, p. 580–583, https://doi.org/10.1038/nature04505.

Leake, B.E., Woolley, A.R., Arps, C.E., Birch, W.D., Gilbert, M.C., Grice, J.D., and Krivovichev, V.G., 1997, Nomenclature of amphiboles; Report of the subcommittee on amphiboles of the International Mineralogical Association, Commission on New Minerals and Mineral Names: Canadian Mineralogist, v. 35, p. 219–246, https://doi.org/10.1180/minmag.1997.061.405.13.

Leech, M.L., 2001, Arrested orogenic development: Eclogitization, delamination, and tectonic collapse: Earth and Planetary Science Letters, v. 185, no. 1–2, p. 149–159, https://doi.org/10.1016/S0012-821X(00)00374-5.

Li, S.G., Xiao, Y.L., Liou, D.L., Chen, Y.Z., Ge, N.J., Zhang, Z.Q., Sun, S.S., Cong, B.L., Zhang, R.Y., Hart, S.R., and Wang, S.S., 1993, Collision of the North China and Yangtse Blocks and formation of coesite-bearing eclogites: Timing and processes: Chemical Geology, v. 109, no. 1–4, p. 89–111, https://doi.org/10.1016/0009-2541(93)90063-O.

Li, S.G., Hong, J.A., Li, H.M., and Jiang, L.L., 1999, Zircon U-Pb datings of pyroxenite-gabbro intrusions in the Dabie orogen and their geological implications [in Chinese with English abstract]: Earth Sciences-Journal of China University of Geosciences, v. 5, no. 3, p. 351–355.

Li, S.G., Huang, F., and Li, H., 2002, Post-collisional lithosphere delamination of the Dabie-Sulu orogen: Chinese Science Bulletin, v. 47, no. 3, p. 259–233, https://doi.org/10.1360/02tb9063.

Li, S.G., He, Y.S., and Wang, S.J., 2013, Process and mechanism of mountain-root removal of the Dabie Orogen: Constraints from geochronology and geochemistry of post-collisional igneous rocks: Chinese Science Bulletin, v. 58, p. 4411–4417, https://doi.org/10.1007/s11434-013-6065-y.

Li, X.P., Zheng, Y.F., Wu, Y.B., Chen, F., Gong, B., and Li, Y.L., 2004, Low-T eclogite in the Dabie terrane of China: Petrological and isotopic constraints on fluid activity and radiometric dating: Contributions to Mineralogy and Petrology, v. 148, p. 443–470, https://doi.org/10.1007/s00410-004-0616-9.

Li, Y., Liu, Y.C., Yang, Y., Rolfo, F., and Groppo, C., 2020a, Petrogenesis and tectonic significance of Neoproterozoic meta-basites and meta-granitoids within the central Dabie UHP zone, China: Geochronological and geochemical constraints: Gondwana Research, v. 78, p. 1–19, https://doi.org/10.1016/j.gr.2019.08.005.

Li, Y., Yang, Y., Liu, Y.C., Groppo, C., and Rolfo, F., 2020b, Muscovite dehydration melting in silica-undersaturated systems: A case study from corundum-bearing anatectic rocks in the Dabie orogen: Minerals (Basel), v. 10, no. 3, p. 213, https://doi.org/10.3390/min10030213.

Liu, Q.S., and Gao, S., 1992, Geophysical properties of the lower crustal granulites from the Qinling orogenic belt, China: Tectonophysics, v. 204, no. 3–4, p. 401–408, https://doi.org/10.1016/0040-1951(92)90318-Z.

Liu, X.Q., Yan, J., and Yang, G., 2020, Geochronology and geochemistry of the Sikongshan intrusion in the Dabie Orogen, Central China: Implication for Mesozoic geodynamic background: Geological Journal, v. 55, no. 4, p. 3010–3035, https://doi.org/10.1002/gj.3536.

Liu, Y.C., and Li, S., 2008, Detachment within subducted continental crust and multi-slice successive exhumation of ultrahigh-pressure metamorphic rocks: Evidence from the Dabie-Sulu orogenic belt: Chinese Science Bulletin, v. 53, p. 3105–3119, https://doi.org/10.1007/s11434-008-0387-1.

Liu, Y.C., and Zhang, C.W., 2020, Exhumation of deeply subducted crust: Review and outlook: Science China. Earth Sciences, v. 63, p. 1904–1924, https://doi.org/10.1007/s11430-019-9639-9.

Liu, Y.C., Li, S., Xu, S., Jahn, B.M., Zheng, Y.F., Zhang, Z., Jiang, L., Chen, G., and Wu, W., 2005, Geochemistry and geochronology of eclogites from the northern Dabie Mountains, central China: Journal of Asian Earth Sciences, v. 25, no. 3, p. 431–443, https://doi.org/10.1016/j.jseaes.2004.04.006.

Liu, Y.C., Li, S.G., Gu, X.F., Xu, S.T., and Chen, G.B., 2007a, Ultrahigh-pressure eclogite transformed from mafic granulite in the Dabie orogen, east-central China: Journal of Metamorphic Geology, v. 25, no. 9, p. 975–989, https://doi.org/10.1111/j.1525-1314.2007.00739.x.

Liu, Y.C., Li, S.G., and Xu, S.T., 2007b, Zircon SHRIMP U-Pb dating for gneisses in northern Dabie high T/P metamorphic zone, central China: Implications for decoupling within subducted continental crust: Lithos, v. 96, no. 1–2, p. 170–185, https://doi.org/10.1016/j.lithos.2006.09.010.

Liu, Y.C., Gu, X.F., Li, S.G., Hou, Z.H., and Song, B., 2011a, Multistage metamorphic events in granulitized eclogites from the North Dabie complex zone, central China: Evidence from zircon U-Pb age, trace element and mineral inclusion: Lithos, v. 122, no. 1–2, p. 107–121, https://doi.org/10.1016/j.lithos.2010.12.005.

Liu, Y.C., Gu, X., Rolfo, F., and Chen, Z., 2011b, Ultrahigh-pressure metamorphism and multistage exhumation of eclogite from the Luotian dome, North Dabie Complex Zone (central China): Evidence from mineral inclusions and decompression textures: Journal of Asian Earth Sciences, v. 42, no. 4, p. 607–617, https://doi.org/10.1016/j.jseaes.2010.10.016.

Liu, Y.C., Deng, L.P., Gu, X.F., Groppo, C., and Franco, R., 2015, Application of Ti-in-zircon and Zr-in-rutile thermometers to constrain high-temperature metamorphism in eclogites from the Dabie orogen, central China: Gondwana Research, v. 27, no. 1, p. 410–423, https://doi.org/10.1016/j.gr.2013.10.011.

Liu, Y.C., Liu, L.X., Li, Y., Gu, X.F., and Song, B., 2017, Zircon U-Pb geochronology and petrogenesis of metabasites from the western Beihuaiyang zone in the Hong'an orogen, central China: Implications for detachment within subducting continental crust at shallow depths: Journal of Asian Earth Sciences, v. 145, p. 74–90, https://doi.org/10.1016/j.jseaes.2016.12.021.

Liu, Y.S., Hu, Z.C., Gao, S., Günther, D., Xu, J., Gao, C.G., and Chen, H.H., 2008, In situ analysis of major and trace elements of anhydrous minerals by LA-ICP-MS without applying an internal standard: Chemical Geology, v. 257, no. 1–2, p. 34–43, https://doi.org/10.1016/j.chemgeo.2008.08.004.

Liu, Y.S., Hu, Z.C., Zong, K.Q., Gao, C.G., Gao, S., Xu, J., and Chen, H.H., 2010, Reappraisement and refinement of zircon U-Pb isotope and trace element analyses by LA-ICP-MS: Chinese Science Bulletin, v. 55, no. 15, p. 1535–1546, https://doi.org/10.1007/s11434-010-3052-4.

Ludwig, K.R., 2003, User's Manual for Isoplot 3.00: A Geochronological Toolkit for Microsoft Excel: Berkeley Geochronology Center Special Publication, v. 4, 70 p.

Lustrino, M., 2005, How the delamination and detachment of lower crust can influence basaltic magmatism: Earth-Science Reviews, v. 72, no. 1–2, p. 21–38, https://doi.org/10.1016/j.earscirev.2005.03.004.

Ma, C.Q., Yang, K.G., Ming, H.L., and Lin, G.C., 2003, The age of transformation for the Mesozoic crust of the Dabie orogen from compression to extension: Evidences from granites: Science in China. Series D, Earth Sciences, v. 33, no. 9, p. 817–827.

Malaspina, N., Hermann, J., Scambelluri, M., and Compagnoni, R., 2006, Multistage metasomatism in ultrahigh-pressure mafic rocks from the North Dabie Complex (China): Lithos, v. 90, no. 1–2, p. 19–42, https://doi.org/10.1016/j.lithos.2006.01.002.

Martin, H., Smithies, R.H., Rapp, R., Moyen, J.F., and Champion, D., 2005, An overview of adakite, tonalite–trondhjemite–granodiorite (TTG), and sanukitoid: Relationships and some implications for crustal evolution: Lithos, v. 79, no. 1–2, p. 1–24, https://doi.org/10.1016/j.lithos.2004.04.048.

Meissner, R., Tilmann, F., and Haines, S., 2004, About the lithospheric structure of central Tibet, based on seismic data from the INDEPTH III profile: Tectonophysics, v. 380, no. 1–2, p. 1–25, https://doi.org/10.1016/j.tecto.2003.11.007.

Menegon, L., Pennacchioni, G., and Stünitz, H., 2006, Nucleation and growth of myrmekite during ductile shear deformation in metagranites: Journal of Metamorphic Geology, v. 24, no. 7, p. 553–568, https://doi.org/10.1111/j.1525-1314.2006.00654.x.

Mo, X.X., Hou, Z.Q., Niu, Y.L., Dong, G.C., Qu, X.M., Zhao, Z.D., and Yang, Z.M., 2007, Mantle contributions to crustal thickening during continental collision: Evidence from Cenozoic igneous rocks in southern Tibet: Lithos, v. 96, no. 1–2, p. 225–242, https://doi.org/10.1016/j.lithos.2006.10.005.

Möller, A., O'Brien, P.J., Kennedy, A., and Kröner, A., 2003, Linking growth episodes of zircon and metamorphic textures to zircon chemistry: An example from the ultrahigh-temperature granulites of Rogaland (SW Norway), *in* Vance, D., Müller, W., and Villa, I.M., eds., Geochronology: Linking the Isotopic Record with Petrology and Textures: Geological Society of London Special Paper 220, p. 65–82, https://doi.org/10.1144/GSL.SP.2003.220.01.04.

Myrow, P.M., Hughes, N.C., Paulsen, T.S., Williams, I.S., Parcha, S.K., Thompson, K.R., Bowing, S.A., Peng, S.C., and Ahluwalia, A.D., 2003, Integrated tectonostratigraphic analysis of the Himalaya and implications for its tectonic reconstruction: Earth and Planetary Science Letters, v. 212, no. 3–4, p. 433–441, https://doi.org/10.1016/S0012-821X(03)00280-2.

Nebel, O., Nebel-Jacobsen, Y., Mezger, K., and Berndt, J., 2007, Initial Hf isotope compositions in magmatic zircon from early Proterozoic rocks from the Gawler Craton, Australia: A test for zircon model ages: Chemical Geology, v. 241, no. 1–2, p. 23–37, https://doi.org/10.1016/j.chemgeo.2007.02.008.

Nelson, K.D., 1992, Are crustal thickness variations in old mountain belts like the Appalachians a consequence of lithospheric delamination?: Geology, v. 20, no. 6, p. 498–502, https://doi.org/10.1130/0091-7613(1992)020<0498:ACTVIO>2.3.CO;2.

Newton, R.C., and Manning, C.E., 2000, Quartz solubility in H_2O-NaCl and H_2O-CO_2 solutions at deep crust-upper mantle pressures and temperatures: 2–15 kbar and 500–900°C: Geochimica et Cosmochimica Acta, v. 64, no. 17, p. 2993–3005, https://doi.org/10.1016/S0016-7037(00)00402-6.

O'Brien, P.J., 2001, Subduction followed by collision: Alpine and Himalayan examples: Physics of the Earth and Planetary Interiors, v. 127, no. 1–4, p. 277–291, https://doi.org/10.1016/S0031-9201(01)00232-1.

Okay, A.I., Xu, S.T., and Sengor, A.M.C., 1989, Coesite from the Dabie Shan eclogites, central China: European Journal of Mineralogy, v. 1, p. 595–598, https://doi.org/10.1127/ejm/1/4/0595.

Patchett, P.J., White, W.M., Feldmann, H., Kielinczuk, S., and Hofmann, A.W., 1984, Hafnium/rare earth element fractionation in the sedimentary system and crustal recycling into the Earth's mantle: Earth and Planetary Science Letters, v. 69, no. 2, p. 365–378, https://doi.org/10.1016/0012-821X(84)90195-X.

Pfiffner, O.A., Ellis, S., and Beaumount, C., 2000, Collision tectonics in the Swiss Alps: Insight from geodynamic modeling: Tectonics, v. 19, no. 6, p. 1065–1094, https://doi.org/10.1029/2000TC900019.

Raase, P., 1974, Al and Ti contents of hornblende, indicators of pressure and temperature of regional metamorphism: Contributions to Mineralogy and Petrology, v. 45, p. 231–236, https://doi.org/10.1007/BF00383440.

Rapp, R.P., and Watson, E.B., 1995, Dehydration melting of metabasalt at 8–32 kbar: Implications for continental growth and crust-mantle recycling: Journal of Petrology, v. 36, no. 4, p. 891–931, https://doi.org/10.1093/petrology/36.4.891.

Rapp, R.P., Shimizu, N., Norman, M.D., and Applegate, G.S., 1999, Reaction between slab derived melts and peridotite in the mantle wedge: Experimental constraints at 3.8 GPa: Chemical Geology, v. 160, no. 4, p. 335–356, https://doi.org/10.1016/S0009-2541(99)00106-0.

Rey, P., Vanderhaeghe, O., and Teyssier, C., 2001, Gravitational collapse of the continental crust: Definitions, regimes, mechanisms and modes: Tectonophysics, v. 342, no. 3–4, p. 435–449, https://doi.org/10.1016/S0040-1951(01)00174-3.

Rolfo, F., Compagnoni, R., Wu, W.P., and Xu, S.T., 2004, A coherent lithostratigraphic unit in the coesite–eclogite complex of Dabie Shan, China: Geologic and petrologic evidence: Lithos, v. 73, no. 1–2, p. 71–94, https://doi.org/10.1016/j.lithos.2003.10.008.

Rubatto, D., and Gebauer, D., 2000, Use of cathodoluminescence for U-Pb zircon dating by IOM Microprobe: Some examples from the western Alps, *in* Pagel, M., Barbin, V., Blanc, P., and Ohnenstetter, D., eds., Cathodoluminescence in Geosciences: Berlin-Heidelberg, Germany, Springer-Verlag, p. 373–400, https://doi.org/10.1007/978-3-662-04086-7_15.

Rudnick, R.L., 1995, Making continental crust: Nature, v. 378, p. 571–578, https://doi.org/10.1038/378571a0.

Rudnick, R.L., and Fountain, D.M., 1995, Nature and composition of the continental crust: A lower crustal perspective: Reviews of Geophysics, v. 33, no. 3, p. 267–309, https://doi.org/10.1029/95RG01302.

Rudnick, R.L., and Gao, S., 2003, Composition of the Continental Crust, *in* Holland, H.D., and Turekian, K.K., eds., The Crust: Treatise on Geochemistry: Oxford, UK, Elsevier-Pergamon, v. 3, p. 1–64.

Schmid, R., Ryberg, T., and Ratschbacher, L., 2001, Crustal structure of eastern Dabie Shan interpreted from deep reflection and shallow tomographic data: Tectonophysics, v. 333, no. 3–4, p. 347–359, https://doi.org/10.1016/S0040-1951(01)00023-3.

Schmidt, M.W., 1992, Amphibole composition in tonalite as a function of pressure: An experimental calibration of the Al-in-hornblende barometer: Contributions to Mineralogy and Petrology, v. 110, p. 304–310, https://doi.org/10.1007/BF00310745.

Springer, W., and Seck, H.A., 1997, Partial fusion of basic granulites at 5 to 15 kbar: Implications for the origin of TTG magmas: Contributions to Mineralogy and Petrology, v. 127, p. 30–45, https://doi.org/10.1007/s004100050263.

Stern, R.A., and Hanson, G.N., 1991, Archean high-Mg granodiorite: A derivative of light rare earth element enriched monzodiorite of mantle origin: Journal of Petrology, v. 32, no. 1, p. 201–238, https://doi.org/10.1093/petrology/32.1.201.

Sun, S.S., and McDonough, W.F., 1989, Chemical and isotopic systematics of oceanic basalts: Implications for mantle composition and processes: *in* Saunders, A.D., and Norry, M.J., eds., Magmatism in the Ocean Basins: Geological Society of London Special Publication 42, no. 1, p. 313–345, https://doi.org/10.1144/GSL.SP.1989.042.01.19.

Tiepolo, M., Oberti, R., Zanetti, A., Vannucci, R., and Foley, S.F., 2007, Trace-element partitioning between amphibole and Silicate melt: Reviews in Mineralogy and Geochemistry, v. 67, p. 417–452, https://doi.org/10.2138/rmg.2007.67.11.

Touret, J.L.R., and Huizenga, J.M., 2012, Charnockite microstructures: From magmatic to metamorphic: Geoscience Frontiers, v. 3, no. 6, p. 745–753, https://doi.org/10.1016/j.gsf.2012.05.004.

Vanderhaeghe, O., and Teyssier, C., 2001, Partial melting and flow of orogens: Tectonophysics, v. 342, no. 3–4, p. 451–472, https://doi.org/10.1016/S0040-1951(01)00175-5.

Vissers, R.L.M., Platt, J.P., and van der Wal, D., 1995, Late orogenic extension of the Betic Cordillera and the Alboran Domain: A lithospheric view: Tectonics, v. 14, p. 786–803, https://doi.org/10.1029/95TC00086.

von Blanckenburg, F., and Davies, J.H., 1995, Slab breakoff: A model for syncollisional magmatism and tectonics in the Alps: Tectonics, v. 14, no. 1, p. 120–131, https://doi.org/10.1029/94TC02051.

Wang, C.Y., Zeng, R.S., Mooney, W.D., and Hacker, B.R., 2000, A crustal model of the ultrahigh-pressure Dabie Shan orogenic belt, China, derived from deep seismic refraction profiling: Journal of Geophysical Research. Solid Earth, v. 105, no. B5, p. 10857–10869, https://doi.org/10.1029/1999JB900415.

Wang, J.H., and Deng, S.X., 2002, Emplacement age for the mafic-ultramafic plutons in the northern Dabie Mts. (Hubei): Zircon U-Pb, Sm-Nd and $^{40}Ar/^{39}Ar$ dating: Science in China. Series D, Earth Sciences, v. 45, no. 1, p. 1–12.

Wang, Q., Wyman, D.A., Xu, J.F., Jian, P., Zhao, Z.H., Li, C.H., Xu, W., Ma, J.L., and He, B., 2007, Early Cretaceous adakitic granites in the Northern Dabie Complex, central China: Implications for partial melting and delamination of thickened lower crust: Geochimica et Cosmochimica Acta, v. 71, no. 10, p. 2609–2636, https://doi.org/10.1016/j.gca.2007.03.008.

Wang, S.J., Li, S.G., Chen, L.J., He, Y.S., An, S.C., and Shen, J., 2013, Geochronology and geochemistry of leucosomes in the North Dabie Terrane, East China: Implication for post-UHPM crustal melting during exhumation: Contributions to Mineralogy

and Petrology, v. 165, p. 1009–1029, https://doi.org/10.1007/s00410-012-0845-2.

Wang, X., Liou, J.G., and Mao, H.J., 1989, Coesite-bearing eclogites from the Dabie Mountains in central China: Geology, v. 17, no. 12, p. 1085–1088, https://doi.org/10.1130/0091-7613(1989)017<1085:CBEFTD>2.3.CO;2.

Wang, Y.J., Fan, W.M., Peng, T.P., Zhang, H.F., and Guo, F., 2005, Nature of the Mesozoic lithospheric mantle and tectonic decoupling beneath the Dabie Orogen, Central China: Evidence from $^{40}Ar/^{39}Ar$ geochronology, elemental and Sr-Nd-Pb isotopic compositions of early Cretaceous mafic igneous rocks: Chemical Geology, v. 220, p. 165–189, https://doi.org/10.1016/j.chemgeo.2005.02.020.

Whitney, D.L., and Evans, B.W., 2010, Abbreviations for names of rock-forming minerals: The American Mineralogist, v. 95, no. 1, p. 185–187, https://doi.org/10.2138/am.2010.3371.

Williams, I.S., 1998, U-Th-Pb geochronology by ionmicroprobe, *in* McKibben, M.A., Shanks III, W.C., Ridley, W.I., eds., Applications of Microanalytical Techniques to Understanding Mineralizing Processes: Reviews in Economic Geology, v. 7, p. 1–35.

Wolf, M.B., and Wyllie, P.J., 1993, Garnet growth during amphibolite anatexis: Implications of a garnetiferous restite: The Journal of Geology, v. 101, no. 3, p. 357–373, https://doi.org/10.1086/648229.

Wolf, M.B., and Wyllie, P.J., 1994, Dehydration-melting of amphibolite at 10 kbar: The effects of temperature and time: Contributions to Mineralogy and Petrology, v. 115, p. 369–383, https://doi.org/10.1007/BF00320972.

Wu, F.Y., Clift, P.D., and Yang, J.H., 2007a, Zircon Hf isotopic constraints on the sources of the Indus Molasse, Ladakh Himalaya, India: Tectonophysics, v. 26, p. 1029–1044, https://doi.org/10.1029/2006TC002051.

Wu, Y.B., Zheng, Y.F., Zhang, S.B., Zhao, Z.F., Wu, F.Y., and Liu, X.M., 2007b, Zircon U-Pb ages and Hf isotope compositions of migmatite from the North Dabie terrane in China: Constraints on partial melting: Journal of Metamorphic Geology, v. 25, no. 9, p. 991–1009, https://doi.org/10.1111/j.1525-1314.2007.00738.x.

Xu, H.J., and Zhang, J.F., 2017, Anatexis witnessed post-collisional evolution of the Dabie orogen, China: Journal of Asian Earth Sciences, v. 145, p. 278–296, https://doi.org/10.1016/j.jseaes.2017.04.001.

Xu, H.J., Ma, C.Q., and Ye, K., 2007, Early Cretaceous granitoids and their implications for the collapse of the Dabie orogen, eastern China: SHRIMP zircon U-Pb dating and geochemistry: Chemical Geology, v. 240, no. 3–4, p. 238–259, https://doi.org/10.1016/j.chemgeo.2007.02.018.

Xu, H.J., Ma, C.Q., and Ye, K., 2012a, Early Cretaceous low-Mg adakitic granites from the Dabie orogen, eastern China: Petrogenesis and implications for destruction of the over-thickened lower continental crust: Gondwana Research, v. 23, no. 1, p. 190–207, https://doi.org/10.1016/j.gr.2011.12.009.

Xu, H.J., Ma, C.Q., Zhang, J.F., and Ye, K., 2013, Early Cretaceous low-Mg adakitic granites from the Dabie orogen, eastern China: Petrogenesis and implications for destruction of the over-thickened lower continental crust: Gondwana Research, v. 23, no. 1, p. 190–207, https://doi.org/10.1016/j.gr.2011.12.009.

Xu, S.T., Okay, A.I., Ji, S.Y., Sengör, A.M.C., Su, W., Liu, Y.C., and Jiang, L.L., 1992, Diamond from the Dabie Shan metamorphic rocks and its implication for tectonic setting: Science, v. 256, no. 5053, p. 80–82, https://doi.org/10.1126/science.256.5053.80.

Xu, S.T., Liu, Y.C., Chen, G.B., Compagnoni, R., Rolfo, F., He, M.C., and Liu, H.F., 2003, New finding of microdiamonds in eclogites from Dabie-Sulu region in central-eastern: Chinese Science Bulletin, v. 48, p. 988–994, https://doi.org/10.1007/BF03184213.

Xu, S.T., Liu, Y.C., Chen, G.B., Ji, S.Y., Ni, P., and Xiao, W.S., 2005, Microdiamonds, their classification and tectonic implications for the host eclogites from the Dabie and Su-Lu regions in central eastern China: Mineralogical Magazine, v. 69, no. 4, p. 509–520, https://doi.org/10.1180/0026461056940267.

Xu, S.T., Wu, W.P., Lu, Y.Q., and Wang, D.H., 2012b, Tectonic setting of the low-grade metamorphic rocks of the Dabie Orogen, central eastern China: Journal of Structural Geology, v. 37, p. 134–149, https://doi.org/10.1016/j.jsg.2012.01.020.

Xue, F., Rowley, D.B., Tucker, R.D., and Peng, Z., 1997, U-Pb zircon ages of granitoid rocks in the north Dabie Complex, eastern Dabie Shan, China: The Journal of Geology, v. 105, p. 744–753, https://doi.org/10.1086/515984.

Yang, W.C., 2002, Geophysical profiling across the Sulu ultra-high-pressure metamorphic belt, eastern China: Tectonophysics, v. 354, no. 3–4, p. 277–288, https://doi.org/10.1016/S0040-1951(02)00386-4.

Yang, Y., Liu, Y.C., Li, Y., Croppo, C., and Rolfo, F., 2020, Zircon U-Pb dating and petrogenesis of multiple episodes of anatexis in the North Dabie complex zone, central China: Minerals (Basel), v. 10, no. 7, https://doi.org/10.3390/min10070618.

Zhao, Z.F., Zheng, Y.F., Wei, C.S., Wu, Y.B., Chen, F.K., and Jahn, B.M., 2005, Zircon U-Pb age, element and C-O isotope geochemistry of post-collisional mafic-ultramafic rocks from the Dabie orogen in east-central China: Lithos, v. 83, no. 1–2, p. 1–28, https://doi.org/10.1016/j.lithos.2004.12.014.

Zhao, Z.F., Zheng, Y.F., Wei, C.S., and Wu, Y.B., 2007, Post-collisional granitoids from the Dabie orogen in China: Zircon U-Pb age, element and O isotope evidence for recycling of subducted continental crust: Lithos, v. 93, no. 3–4, p. 248–272, https://doi.org/10.1016/j.lithos.2006.03.067.

Zhao, Z.F., Zheng, Y.F., Wei, C.S., Chen, F.K., Liu, X.M., and Wu, F.Y., 2008, Zircon U-Pb ages, Hf and O isotopes constrain the crustal architecture of the ultrahigh-pressure Dabie orogen in China: Chemical Geology, v. 253, p. 222–242, https://doi.org/10.1016/j.chemgeo.2008.05.011.

Zhao, Z.F., Zheng, Y.F., Wei, C.S., and Wu, F.Y., 2011, Origin of postcollisional magmatic rocks in the Dabie orogen: Implications for crust–mantle interaction and crustal architecture: Lithos, v. 126, no. 1–2, p. 99–114, https://doi.org/10.1016/j.lithos.2011.06.010.

Science Editor: Rob Strachan
Associate Editor: Jeff Hannon

Manuscript Received 18 May 2021
Revised Manuscript Received 22 August 2021
Manuscript Accepted 29 September 2021

Printed in the USA